each clone was analyzed by Western blotting as described below.

Adenoviral Expression of Myc-GLUT4-ECFP in C2C12 Cells—An adenoviral technique was used to express rat GLUT4, possessing the c-Myc epitope tag in the first extracellular loop and enhanced cyan fluorescent protein (ECFP) at the C terminus. Briefly, established exofacial-Myc-GLUT4-ECFP cDNA (32) was inserted into adenoviral vector pHMCA5, generously provided by Dr. H. Mizuguchi (33, 34). The high titer viruses were produced by transfection of pHMCA5-Myc-GLUT4-ECFP or empty vector into 293 cells using FuGENE 6 transfection reagents (Roche Applied Science). Viral stocks of $5–50 \times 10^7$ plaque-forming units/ml were prepared in serum-free DMEM and frozen at −80 °C. The next day the medium was changed, and incubation was continued for another 24 h. Then, 2-deoxy[^{3}H]glucose and Myc antibody uptake assays were performed as described below. Expression of Myc-GLUT4-ECFP was confirmed by Western blotting and immunofluorescent staining.

Western Blot Analysis—The expression levels of each protein were analyzed by Western blotting. In brief, cells were lysed with NET buffer (50 mM Tris-HCl, pH 7.4, 150 mM NaCl, 1 mM EDTA, 1% Triton X-100, 0.1% SDS, 100 units/ml aprotinin, 1 mM phenylmethylsulfonyl fluoride, 5 μg/ml leupeptin, and 5 μg/ml pepstatin A). The extracts were centrifuged at 13,000 × *g* for 10 min at 4 °C to remove insoluble materials. The protein concentrations of supernatants were determined, and 3× Laemmli sample buffer was added to achieve a 1× final concentration. From 50 to 100 μg of total protein was subjected to 7.5–10% SDS-PAGE (1:30, bis:acrylamide). Proteins were transferred to a polyvinylidene difluoride membrane (Immobilon-P, Millipore Corp.), and the membranes were then blocked for 2 h at room temperature with 5% BSA in Tris-buffered saline (TBS) containing 0.1% Tween 20. Immunoblotting to detect each protein was achieved with an overnight incubation at 4 °C with 3% BSA/TBS containing either anti-sortilin antibody (1:1000), anti-myosin heavy chain (MHC) antibody (1:1000), anti-myogenin antibody (1:1000), anti-sarcomeric α-actinin antibody (1:1000), or anti-troponin T antibody (1:1000). Anti-β-actin (1:500) or anti-insulin receptor β-subunit (1:1000) antibodies were used as a loading control. Specific total proteins were visualized after subsequent incubation with a 1:5000 dilution of anti-mouse or anti-rabbit IgG conjugated to horseradish peroxidase and a SuperSignal Chemiluminescence detection procedure (Pierce). Protein concentrations were determined using a bicinchoninic acid (BCA) protein assay kit (Pierce). Three independent experiments were performed for each condition.

2-Deoxyglucose Uptake Assay—A 2-deoxy[^{3}H]glucose uptake assay was performed as previously described (35). Briefly, cells were starved in serum-free DMEM for 4 h, and then washed with Krebs-Ringer phosphate HEPES buffer (KRPH buffer; 10 mM phosphate buffer, pH 7.4, 1 mM $MgSO_4$, 1 mM $CaCl_2$, 136 mM NaCl, 4.7 mM KCl, 10 mM HEPES (pH 7.6)). The serum-starved cells were incubated without or with 100 nM insulin for 60 min in KRPH buffer and then chilled on ice. After washing with ice-cold KRPH buffer, glucose transport was determined by addition of 2-deoxy[^{3}H]glucose (PerkinElmer Life Sciences, 0.1 mM, 0.5 μCi/ml). After 4 min of incubation with the KRPH buffer containing 2-deoxy[^{3}H]glucose, the reaction was stopped by adding phosphate-buffered saline (PBS) containing 10 μM cytochalasin B (Sigma), and the cells were washed three times with ice-cold PBS. The cells were then lysed in 0.2 N NaOH solution, and 2-deoxy[^{3}H]glucose uptake was assessed by scintillation counting. 20 μM cytochalasin B were added to the assay buffer for the measurement of nonspecific background. Specific uptake, *i.e.* the background subtracted from the total uptake, was obtained. The protein content was determined in each experiment with a BCA protein assay kit. Data are presented as picomoles of 2-deoxy[^{3}H]glucose per milligram protein per minute. For each experiment, at least three assays were performed under each condition, and each experiment was repeated at least three times.

Anti-Myc Antibody Uptake Assay—For the measurement of insulin-induced GLUT4 translocation, the C2C12 cells expressing Myc-GLUT4-ECFP were starved in serum-free DMEM for 4 h, washed three times with KRPH buffer, and then placed in a CO_2 incubator with 2 ml of KRPH buffer. Ten minutes after incubation, the cells were treated with or without 100 nM insulin in the presence of 4 μg/ml of the anti-Myc antibody for 60 min. Next, the cells were washed three times with ice-cold PBS, harvested using 1× Laemmli sample buffer without bromphenol blue and 2-mercaptoethanol (2-ME). After the protein concentration had been determined, bromphenol blue and 2-mercaptoethanol were added, denatured by incubation for 5 min at 95 °C, and subjected to Western blotting using anti-mouse IgG antibody, anti-Myc antibody, or anti-Sortilin antibody.

Immunofluorescence and Image Analysis—After experimental treatments, the cells were washed in PBS and fixed for 20 min in 2% paraformaldehyde/PBS containing 0.1% Triton X-100. The cells were washed, and then blocked in PBS containing 5% calf serum plus 1% BSA for 1 h at room temperature. Primary and secondary antibodies were used at 1:100 and 1:1000 dilutions, respectively (unless otherwise indicated), in 1% BSA/PBS, and samples were mounted on glass slides with Vectashield (Vector Laboratories, Burlingame, CA). Cells were imaged using a confocal fluorescence microscope (Olympus Fluoview FV-1000) with associated application program ASW Ver. 1.3 (Olympus, Tokyo, Japan). Images were then imported into Adobe Photoshop (Adobe Systems, Inc.) for processing. Myogenin-positive cells were counted within a 500-μm × 500-μm area. At least five fields were counted for each sample under 20× microscopic magnification. For all microscopic analyses, at least three independent experiments were performed for each condition.

Subcellular Fractionation of C2C12 Cells—To detect endogenous GLUT1 and GLUT4, fractionation was performed according to the method of Tortorella and Pilch (36). Briefly, cells (three 150-mm plates for each sample) were washed with PBS three times, harvested with a cell scraper, suspended in 0.25 M sucrose, 20 mM Hepes-HCl (pH 7.4), 1 mM EDTA, 1 μg/ml aprotinin, 1 μg/ml pepstatin, 1 μg/ml leupeptin, and 1 mM phenylmethylsulfonyl fluoride, then homogenized with a Teflon glass homogenizer. The homogenate was centrifuged at 600 × *g* for 10 min at 4 °C. The supernatant was centrifuged at

100,000 × *g* for 1 h to collect the pellet for the total membrane fraction. For detection of GLUT1, the total membrane fraction was lysed in 100 μl of 1× Laemmli sample buffer, and subjected to Western blotting using anti-GLUT1 antibody (1:5840). For detection of GLUT4, the total membrane fraction was lysed in 100 μl of 8 M urea, 5% SDS, and 50 mM Tris-HCl (pH 6.8). After the protein concentration had been determined as described above, dithiothreitol and bromphenol blue were added to each sample (final concentrations, 343.6 μM and 0.005%, respectively). After incubation for 30 min at 37 °C, samples were subjected to SDS-PAGE followed by immunoblotting using anti-GLUT4 antibody (1:500) (37).

Real-time Reverse Transcription-PCR—Total RNA was prepared using TRIzol reagent according to the manufacturer's instructions and was quantified using an ND-1000 spectrophotometer (NanoDrop Technologies, Wilmington, DE). Reverse transcription was carried out using the First Strand cDNA Synthesis kit for PCR from Roche Applied Science. Real-time PCR reactions were performed using the Roche LightCycler, utilizing Roche SYBR Green reagents according to the manufacturer's instructions. Amplification of PCR products was quantified during PCR by measuring fluorescence associated with binding of double-stranded DNA to the SYBR Green dye incorporated into the reaction mixture. The sequences of the oligonucleotides used to PCR-amplify the cDNAs of interest were: GLUT4 (upper primer, 5′-TGCTCTCCTGCAGCTGATT-3′; lower primer, 5′-TTCAGCTCAGCTAGTGCGTC-3′), GLUT1 (upper primer, 5′-CTTCCTGCTCATCAATCGT-3′; lower primer, 5′-AGCTCCAAGATGGTGACCTT-3′), sortilin (upper primer, 5′-AATGGTCGAGACTATGTTGTG-3′; lower primer, 5′-CCGGTACCCATTTGTTGT-3′), and Ubc9 (upper primer, 5′-GGCACAATGAACCTGATGAAC-3′; lower primer, 5′-TTGGTGGTGAGGACGGATAGT-3′). Glyceraldehyde-3-phosphate dehydrogenase was quantified as a housekeeping gene by using: upper primer 5′-GGAGAAACCTGCCAAGTATGA-3′, and lower primer 5′-GCATCGAAGGTGGAAGAGT-3′. Following an initial denaturation step of 95 °C for 1 min, 30–45 cycles of 95 °C for 10 s, 60 °C for 1 s, and 72 °C for 10 s were used for GLUT4, GLUT1, sortilin, and Ubc9. For glyceraldehyde-3-phosphate dehydrogenase, an initial denaturation step of 95 °C for 10 min, followed by 45 cycles of 95 °C for 10 s, 57.5 °C for 15 s, and 72 °C for 15 s was used.

siRNA-mediated Reduction of Sortilin in C2C12 Cells—The siRNA species purchased from Nippon EGT Co. Ltd. (Toyama, Japan) were designed to target the following cDNA sequences: scrambled, 5′-AGGGUGGGUUUGGCCAAAATT-3′; and sortilin siRNA-1, 5′-GGUGGUGUUAACAGCAGAGTT-3′; sortilin siRNA-2, 5′-CCAUUGGUGUGAAAAUCUA-3′, and sortilin siRNA-3, 5′-GGACCACAUUACUAUACCA-3′. Scramble and sortilin siRNA-1 were modified from the reference (38), and the sequences of sortilin siRNA-2 and -3 were provided by Nippon EGT Co. Ltd. 200 nmol of sortilin siRNA, or scrambled siRNA species, was introduced into C2C12 myoblasts using Oligofectamine (Invitrogen). Ninety-six hours after transfection (day 3 of differentiation), cells were harvested with NET buffer followed by SDS-PAGE and immunoblotting using anti-sortilin antibody, anti-myogenin antibody, or anti-β-actin antibody (as a control).

Measurement of GLUT Stability—Adenoviral infected WT- and sort10-C2C12 cells expressing Myc-GLUT4-ECFP were treated with 10 μg/ml cycloheximide, and the cells were then harvested with NET buffer at the indicated time intervals. Cell lysates were subjected to SDS-PAGE, followed by Western blotting analysis using anti-GLUT1 or anti-Myc antibody.

Statistical Analysis—Results are expressed as means ± S.E., and the data were analyzed by analysis of variance followed by Student's *t* test. Differences were considered to be significant at *, $p < 0.05$; **, $p < 0.01$; and ***, $p < 0.001$.

RESULTS

Sortilin Expression during Differentiation of C2C12 Cells—To investigate the physiological role of sortilin in C2C12 myocytes, we first determined changes in expression levels of sortilin during myogenesis of C2C12 cells by Western blotting (Fig. 1*A*, *upper panel*). Sortilin was undetectable in undifferentiated C2C12 myoblasts (Day 0) but was observed as a ~100-kDa protein at Day 2 of differentiation when these myoblasts were differentiated in a differentiation medium containing 5 mM glucose. The amount of sortilin then gradually increased until Day 5 and remained unchanged up to Day 8. As a control for myogenic differentiation, expression levels of myogenin (*middle panel*) and MHC (*lower panel*) were also determined. Immunofluorescent staining demonstrated sortilin containing endosomes to be located throughout the cytoplasm. Thus, colocalizations with GLUT4 (*panels a* and *b*, *red*), cation-independent mannose 6-phosphate/insulin-like growth factor-2 receptor (*panels c* and *d*, *red*), and Syntaxin 6 (*panels e* and *f*, *red*) were obvious, although the sortilin-positive endosomes were apparently devoid of p115 (*panels g* and *h*, *red*), a *cis*-Golgi marker in differentiated C2C12 myotubes.

Expression of Sortilin Induces Spontaneous Myogenic Differentiation of C2C12 Cells—To explore the functional roles of sortilin in C2C12 myocytes, we established C2C12 cells in which sortilin is stably expressed using a retroviral technique. In the process of isolating positive clones, we unexpectedly found that overexpression of sortilin in C2C12 myoblasts often resulted in spontaneous myotubular formation even in growth medium containing 10% fetal bovine serum (data not shown). Twenty clones of drug-resistant C2C12 cells were isolated, nine of which stably expressed sortilin as assessed by Western blotting analysis. All nine clones expressing detectable levels of exogenous sortilin displayed the myotubular phenotype once they reached confluence. Three independent clones expressing sortilin, two control clones expressing empty vector, and parental wild-type cells were further analyzed. As shown in Fig. 2, in growth medium, neither wild-type C2C12 (WT-C2C12) nor the control clone expressing empty vector expressed sortilin (Fig. 2*A*, *right panel*, *lanes 1* and 2). Furthermore, neither displayed a myotubular phenotype even after reaching confluence (Fig. 2*A*, *panels a* and *b*). In sharp contrast, C2C12 clones expressing exogenous sortilin (Sort10- and Sort15-C2C12) (Fig. 2, *right panel*, *lanes 3* and *4*) underwent spontaneous differentiation as evidenced by myotube formation (Fig. 2*A*, *left panels*, *panels c* and *d*). Immunofluorescent analysis revealed that even before differentiation began Sort10-C2C12 cells already expressed various muscle differentiation markers,

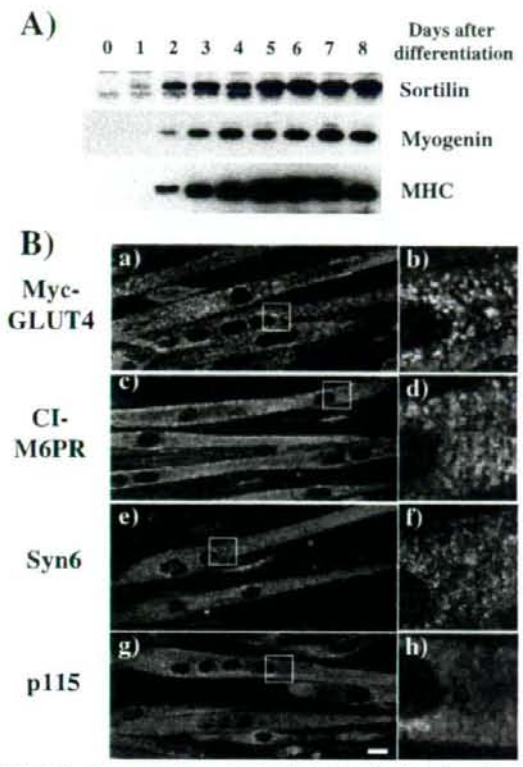

FIGURE 1. **Protein expression and subcellular localization of sortilin during C2C12 differentiation.** *A*, C2C12 myoblasts were differentiated in conventional differentiation medium (DMEM containing 5 mM glucose plus 2% calf serum). The differentiation medium was changed every 24 h. Whole cell lysates were obtained daily until day 8 of differentiation. Total protein extracts (22.5 μg/lane) were subjected to SDS-PAGE followed by Western blot analysis using anti-sortilin (*upper panel*), anti-myogenin (*middle panel*), and anti-myosin heavy chain (MHC; *lower panel*) antibodies. *B*, differentiated C2C12 myotubes (Day 6) were fixed and subjected to immunofluorescent staining using rabbit anti-sortilin antibody (*green*) with either mouse monoclonal anti-Myc (*panels a* and *b*), anti-cation-independent mannose 6-phosphate/insulin-like growth factor-2 receptor (*panels c* and *d*), anti-syntaxin 6 (*panels e* and *f*), or anti-p115 (*panels g* and *h*) antibodies (*red*). For examining co-localization between sortilin and GLUT4 (*panels a* and *b*), Myc-GLUT4-ECFP was transiently expressed by infecting C2C12 cells at Day 4 of differentiation with the adenovirus containing the Myc-GLUT4-ECFP gene and then subjecting these cells to immunofluorescent analysis at 2 days after infection (Day 6 of differentiation). Fluorescence signals were detected under confocal microscopy. The *squares* indicated in *panels a*, *c*, *d*, and *g* were magnified and are shown in the *right panels*. *Images* are representative fields of view from three independent experiments. *Scale bar* = 10 μm.

including myogenin (Fig. 2*B*, *panel d*), MHC (Fig. 2, *panel e*), and titin (Fig. 2, *panel f*), observations not made in either WT-C2C12 cells (Fig. 2*B*, *panels a–c*) or empty vector-expressing C2C12 cells (Fig. 2*B*, *panels d–f*). Essentially the same results were obtained in the other clones overexpressing sortilin, but not in other control C2C12 clone obtained by infection with empty retrovirus lacking an insert, and levels of sortilin protein in the control cells were not significantly different from those observed in the non-infected C2C12 myocytes (data not shown).

This stimulatory effect of sortilin overexpression on myogenesis was further confirmed by Western blot analysis using antibodies against various muscle differentiation marker proteins, including MHC, sarcomeric α-actinin, troponin T, and myogenin (Fig. 2*C*). Even at Day 0, Sort10-C2C12 cells already showed considerable elevations of all muscle differentiation marker proteins tested (*lane 2*), observations not made in WT-C2C12 cells (*lane 1*). At Day 4 of differentiation, all of these differentiation marker proteins were also detected in WT-C2C12 cells, although their expression levels were obviously lower in these (*lane 3*) than in Sort10-C2C12 cells (*lane 4*). At Day 7 of differentiation, most of these expressions reached comparable levels in WT-C2C12 (*lane 5*) and Sort10-C2C12 (*lane 6*) cells. Together, these data clearly demonstrate that sortilin overexpression in C2C12 myoblasts results in spontaneous myogenic differentiation once confluence is reached even under growth stimulating conditions.

Involvement of the proNGF-p75NTR Autocrine Loop in the Spontaneous Differentiation of Sortilin-overexpressing C2C12 Cells—Since recent studies have revealed direct interactions among sortilin, p75NTR, and proNGF exerting biological effects in neuronal cells (22, 25), we examined the possible involvement of proNGF and p75NTR, the existence of which in C2C12 cells was previously reported (26, 27), in the process of spontaneous differentiation induced by sortilin overexpression. To address this question, Sort10-C2C12 cells were cultured in the presence or absence of a p75NTR-neutralizing antibody that blocks p75NTR-mediated biological responses (39). The p75NTR-neutralizing antibody significantly reduced the number of Sort10-C2C12 myocytes expressing myogenin in the growth medium, whereas control mouse IgG had no such effect (Fig. 3*A*, *left panel*). In addition, essentially the same result was obtained when an NGF-neutralizing antibody that blocks both NGF and proNGF action was added to the culture instead of the p75NTR-neutralizing antibody (Fig. 3*A*, *right panel*). We also found the anti-p75NTR antibody to be very efficiently endocytosed only in C2C12 cells expressing sortilin (Fig. 3*B*, *panel d*, sortilin; *green*, mouse IgG; *red*), not in control cells expressing empty vector (Fig. 3*B*, *panel b*). No control mouse IgG was incorporated into C2C12 cells, regardless of sortilin expression during the incubation (Fig. 3*B*, *panels a* and *c*). This observation suggests that sortilin overexpression may facilitate complex formation with p75NTR, leading to efficient incorporation of the anti-p75NTR antibody. These data indicate that the stimulatory effect of sortilin overexpression on myogenesis is dependent on the existence of functional p75NTR that has an ability to form the high-affinity proNGF receptor with sortilin.

Physiological Significance of Endogenous Sortilin Expression in Myogenic Differentiation of C2C12 Cells—Because sortilin expression was markedly up-regulated during C2C12 differentiation (Fig. 1), we examined the physiological significance of sortilin expression in the process of myogenic differentiation using the siRNA-mediated gene silencing technique to decrease the expression of endogenous sortilin (Fig. 3*C*). Three of the sortilin sequence-specific siRNA oligonucleotides (*Oligo #1*, *#2*, and *#3*) significantly reduced endogenous sortilin expression at Day 2 of C2C12 differentiation (Fig. 3*C*, *upper panel*, *lanes 1–3*), resulting in a concomitant suppression of myogenin expression (*middle panel*, *lanes 1–3*), whereas a control scramble oligonucleotide had no effect on the expression of

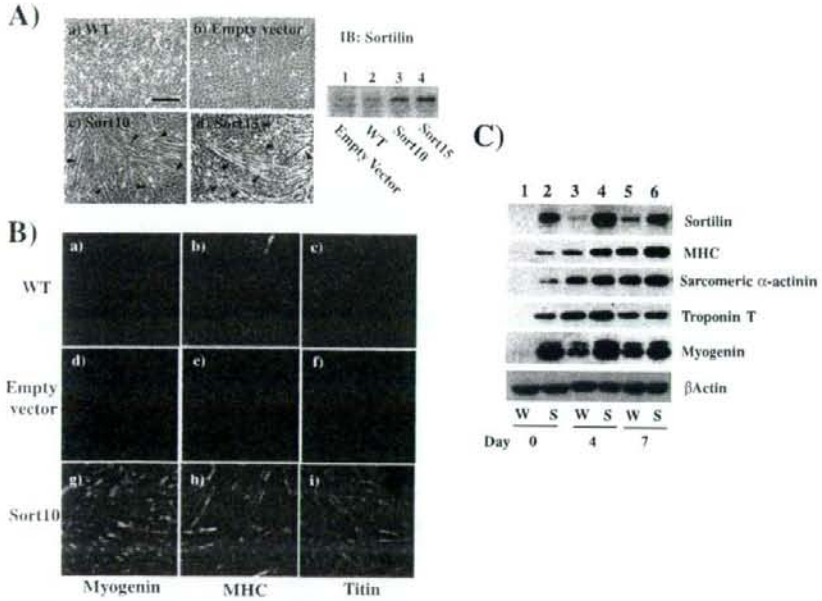

FIGURE 2. **Sortilin overexpression induces spontaneous myogenic differentiation of C2C12 cells.** *A*, parental (WT, *panel a*), empty-vector-expressing (*panel b*) and sortilin-overexpressing (Sort10, *panel c*; Sort15, *panel d*) C2C12 cells were grown to confluence (Day 0). Myotubes are indicated by *arrowheads*. *Images* are representative fields of view from three independent experiments. *Scale bar* = 300 μm. Exogenously expressed sortilin in each C2C12 cell culture was detected by Western blotting analysis (*right panel*). *B*, WT (*panels a–c*), empty vector (*panels d–f*), and Sort10 (*panels g–i*) C2C12 cells at Day 0 were fixed and subjected to immunofluorescent staining using mouse monoclonal anti-myogenin (*panels a, d,* and *g*), anti-MHC (*panels b, e,* and *h*), and anti-titin (*panels c, f,* and *i*) antibodies, which were visualized with Alexa488-conjugated secondary antibody (*green*). Nuclei were stained by 4′,6-diamidino-2-phenylindole (*blue*). *Images* are representative fields of view from three independent experiments. *C*, whole cell lysates were obtained from WT (*lanes 1, 3,* and *5*) and Sort10 (*lanes 2, 4,* and *6*) C2C12 cells on the indicated days after differentiation and total protein extracts (25 μg/lane) were subjected to Western blot analysis using antibodies against sortilin, MHC, sarcomeric α-actinin, troponin T, and myogenin. β-Actin was used as a loading control. These are representative immunoblots obtained from three independent experiments.

either sortilin or myogenin (*lane 4*). β-Actin, used as a loading control, was unaffected by siRNA introduction (*lower panel*). In addition, consistent with the sortilin overexpression experiments (Fig. 3*A*), either p75NTR- or NGF-neutralizing antibody also significantly inhibited the conventional differentiation process of wild-type C2C12 cells in a low serum differentiation medium (Fig. 3*D*). These data indicate that endogenous sortilin up-regulated during myogenesis is directly involved in the myogenic differentiation of C2C12 cells, a process possibly mediated through the proNGF-p75NTR autocrine loop.

Involvement of ROCK in the Spontaneous Differentiation of Sortilin-overexpressing C2C12 Cells—Since the p75NTR has been shown to activate the small G-protein Rho and its downstream effector ROCK in various cell types (40, 41), we examined whether this signaling cascade is involved in the spontaneous differentiation of sortilin-overexpressing C2C12 cells (Fig. 3*E*). The myogenin expression observed in sortilin-overexpressing C2C12 cells at Day 0 was diminished when the cells were cultured for 24 h in the presence of an inhibitor of ROCK, Y27632 (Fig. 3*E*, *lower panel*).

Overexpression of Sortilin Contributes to Development of an Insulin-induced Glucose Transport System in C2C12 Cells—To assess whether an insulin-responsive glucose transport system develops in skeletal muscle C2C12 cells under the same conditions as previously reported (12), WT- and Sort10-C2C12 myoblasts expressing Myc-GLUT4-ECFP were obtained using an adenoviral vector, and 2-deoxy[^{3}H]glucose (Fig. 4) and Myc Ab (Fig. 5) uptake assays (35) were then performed. Because Sort10-C2C12 cells tend to undergo spontaneous myotubular formation, we carried out the assay before they reached confluence (Day −1). Nevertheless, some differentiation markers were already being expressed at this time point (data not shown). Under the conventional 2-deoxy[^{3}H]glucose uptake assay protocol (42), insulin-induced augmentation of 2-deoxy[^{3}H]glucose uptake was not observed in either WT-C2C12 myoblasts (Fig. 4*A*, *WT*) or WT-C2C12 myoblasts expressing exogenous Myc-GLUT4-ECFP (Fig. 4*A*, *WT+G4*). Intriguingly, in Sort10-C2C12 myoblasts, basal 2-deoxy[^{3}H]glucose uptake was remarkably decreased, by ~25% (2.89 ± 0.2 pmol/min/mg of protein) as compared with that of WT-C2C12 myoblasts, whereas Sort10-C2C12 myoblasts failed to display any insulin responsiveness probably due to negligible expression of GLUT4 (Fig. 4*A*, *Sort*). However, consistent with a previous study using 3T3 fibroblasts (12), a slight but significant insulin-stimulated 2-deoxy[^{3}H]glucose uptake (~1.5-fold) was observed in Sort10-C2C12 myoblasts expressing Myc-GLUT4-ECFP (Fig. 4*A*, *Sort+G4*). This occurred concurrently with a small increase in basal 2-deoxy[^{3}H]glucose uptake.

Effects of sortilin overexpression on insulin-induced glucose uptake were also examined in differentiated C2C12 myotubes (Days 5–6) (Fig. 4*B*). Because differentiated C2C12 myotubes contain massive amounts of various muscle proteins such as skeletal muscle type myosins and α-actin, normalization by total protein contents for comparing glucose uptake between myoblasts and myotubes may not directly reflect the actual capacity for glucose transport into individual cells. However, it should be noted that the net amount of 2-deoxy[^{3}H]glucose uptake was remarkably low (1.26 ± 0.1 pmol/min/mg of protein) in differentiated C2C12 myotubes, being nearly 10-fold lower than that in undifferentiated C2C12 myoblasts (Fig. 4, *A* and *B*). Consistent with our previous report (35), insulin-induced 2-deoxy[^{3}H]glucose uptake was marginal even in differentiated C2C12 myotubes (Fig. 4*B*, *WT*) under the conventional uptake assay protocol. The adenovirus-mediated expression of Myc-GLUT4-ECFP

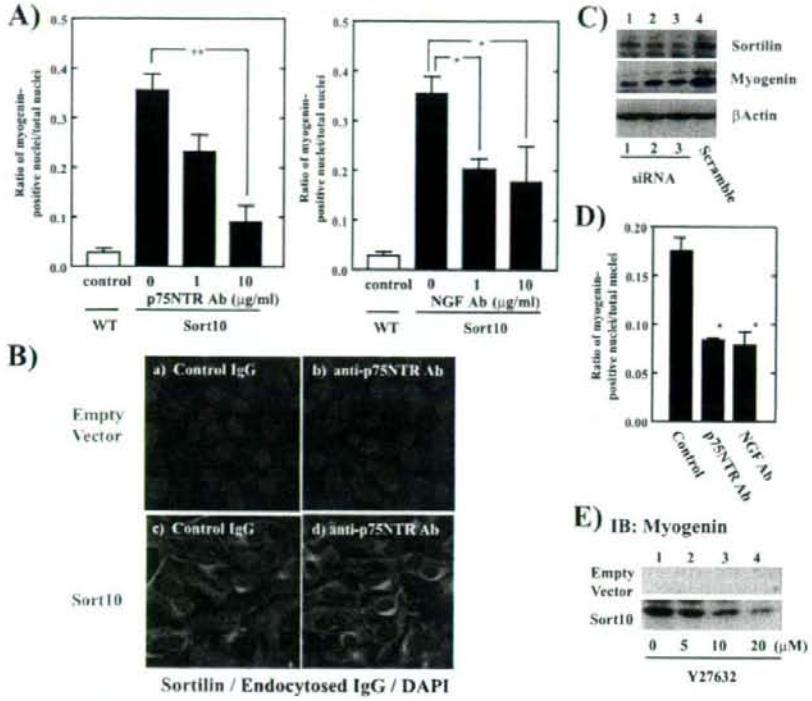

FIGURE 3. **Involvement of sortilin-p75NTR-proNGF autocrine loop in the process of C2C12 differentiation.** *A*, WT (*open bars*) and Sort10 (*solid bars*) C2C12 cells on Day −1 with the addition of either control IgG, anti-p75NTR-neutralizing antibody (*left panel*), or anti-NGF-neutralizing antibody (*right panel*), followed by culture for an additional 24 h. The cells were then fixed and subjected to immunofluorescent staining using mouse monoclonal anti-myogenin visualized with Alexa594-conjugated secondary antibody. Nuclei were stained by 4′,6-diamidino-2-phenylindole, and the number of myogenin positive nuclei was counted. The ratio of myogenin-positive nuclei out of total nuclei was expressed as the mean ± S.E. of four independent experiments. *, $p < 0.05$; **, $p < 0.01$. *B*, empty vector (*panels a* and *b*) or Sort10 (*panels c* and *d*) C2C12 cells seeded in an 8-well slide chamber were treated with 10 μg/ml of anti-p75NTR antibody or mouse IgG before they reached confluence, followed by culture for an additional 24 h. To detect incorporated IgGs, the cells were subjected to immunostaining with anti-mouse IgG (*red*) and anti-sortilin antibody (*green*), as described in A). *C*, WT-C2C12 cells (Day −1) were transfected with siRNA oligonucleotides targeting sortilin (*lanes 1–3*) or control scrambled siRNA oligonucleotide (*lane 4*) by Oligofectamine for 24 h and then cultured in differentiation medium for an additional 3 days. Total protein extracts (135 μg/lane) were subjected to Western blot analysis using anti-sortilin (*upper panel*), anti-myogenin (*middle panel*), or anti-β-actin (*lower panel*) antibodies. *D*, confluent WT-C2C12 cells were cultured in differentiation medium in the absence or presence of 10 μg/ml of either control IgG, anti-p75NTR or anti-NGF antibodies for 48 h. The ratio of myogenin-positive nuclei was assessed by immunostaining analysis as described in *A*. *E*, empty vector (*upper panel*) or Sort10 (*lower panel*) C2C12 cells were incubated with or without the indicated concentrations of Y27632 for 24 h. The whole cell lysates were then subjected to Western blotting analysis using anti-myogenin antibody.

raised 2-deoxy[^{3}H]glucose uptake under both basal and insulin-stimulated conditions, and insulin-responsiveness was slightly improved in differentiated WT-C2C12 myotubes (Fig. 4*B*, *WT+G4*). Consistent with the result obtained in undifferentiated myoblasts expressing sortilin (Fig. 4*A*, *Sort*), differentiated Sort10-C2C12 myotubes showed a further reduction in net 2-deoxy[^{3}H]glucose uptake (Fig. 4*B*, *Sort*). Because of this suppression of basal glucose uptake, a slight but significant augmentation of insulin-induced 2-dexoy[^{3}H]glucose uptake was subsequently seen even without exogenous expression of Myc-GLUT4-ECFP (Fig. 4*B*, *Sort*), presumably reflecting glucose uptake mediated through endogenous GLUT4 translocation in differentiated Sort10-C2C12 myotubes. The adenovirus-mediated expression of Myc-GLUT4-ECFP in Sort10-C2C12 myotubes further enhanced insulin-responsiveness (2.1-fold increase in response to insulin), and this was concurrent with a slight increase in basal 2-deoxy[^{3}H]glucose uptake (Fig. 4*B*, *Sort+G4*).

Effect of Sortilin Overexpression on Insulin-induced GLUT4 Translocation in C2C12 Cells—To confirm that insulin-induced 2-deoxy[^{3}H]glucose uptake was in fact achieved through the translocation of GLUT4 to the plasma membrane, the amount of Myc-GLUT4-ECFP exposed to the cell surface during insulin stimulation was assessed using an anti-Myc antibody (Myc Ab) uptake assay (Fig. 5) (35). The serum-starved WT- or Sort10-C2C12 myotubes expressing Myc-GLUT4-ECFP (Days 5–6) were incubated for 1 h in KRPH buffer containing 4 μg/ml Myc Ab in the absence (Fig. 5, *lanes 1* and *3*) or presence (*lanes 2* and *4*) of insulin (100 nM), and whole cell lysates were then subjected to SDS-PAGE followed by Western blotting using antibodies against anti-mouse IgG for detecting Myc Ab uptake and anti-BD-living colors for detecting the total amount of Myc-GLUT4-ECFP expressed. Consistent with our previous report (35), a small but significant increase in the uptake of Myc Ab was observed with insulin stimulation in WT-C2C12 myotubes expressing Myc-GLUT4-ECFP (Fig. 5, *upper panel*, *lanes 1* and *2*). Importantly, insulin-responsive GLUT4 translocation as assessed by the Myc Ab uptake assay appears to be significantly improved in Sort10-C2C12 myotubes (Fig. 5, *lane 4*), despite marked suppression of net 2-deoxy[^{3}H]glucose uptake in comparison with WT-C2C12 myotubes (Fig. 4*B*). Together, these data clearly demonstrate that sortilin overexpression improves insulin-responsive glucose transport by increasing insulin-responsive GLUT4 translocation in C2C12 myotubes. Our data also indicate the importance of decreased basal glucose uptake in the emergence of markedly increased insulin-responsive glucose uptake.

Effects of Sortilin Overexpression on Expressions of GLUT1 and GLUT4 in C2C12 Cells—Because sortilin overexpression markedly decreased basal glucose uptake (Fig. 5) and also appeared to stimulate C2C12 differentiation (Figs. 1 and 2), we examined protein and mRNA expressions of endogenous GLUT1 and GLUT4 in WT- and Sort10-C2C12 cells during

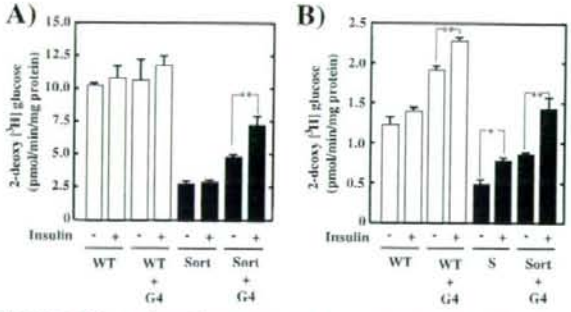

FIGURE 4. **Effects of sortilin overexpression on basal and insulin-stimulated 2-deoxy[^{3}H]glucose uptake in C2C12 cells.** *A*, undifferentiated WT (*open bars, WT*) and Sort10 (*solid bars, Sort*) C2C12 myoblasts were infected with adenovirus containing the Myc-GLUT4-ECFP gene (*G4*) or no insert. Thirty-six hours after infection, the cells were serum starved for 4 h, followed by preincubation with KRPH buffer for 10 min, and then stimulated with or without 100 nM insulin for 60 min. The cells were then subjected to the 2-deoxy[^{3}H]glucose uptake assay as described under "Experimental Procedures." Results were expressed as the mean ± S.E. of three independent experiments. *, $p < 0.05$; **, $p < 0.01$. *B*, WT (*open bars, WT*) and Sort10 (*solid bars, Sort*) C2C12 myotubes at Day 5 of differentiation were infected with adenovirus containing the Myc-GLUT4-ECFP gene (*G4*) or no insert. Thirty-six hours after infection, the cells were subjected to the 2-deoxy[^{3}H]glucose uptake assay as described in *A*. Results were expressed as the mean ± S.E. of three independent experiments. *, $p < 0.05$; **, $p < 0.01$.

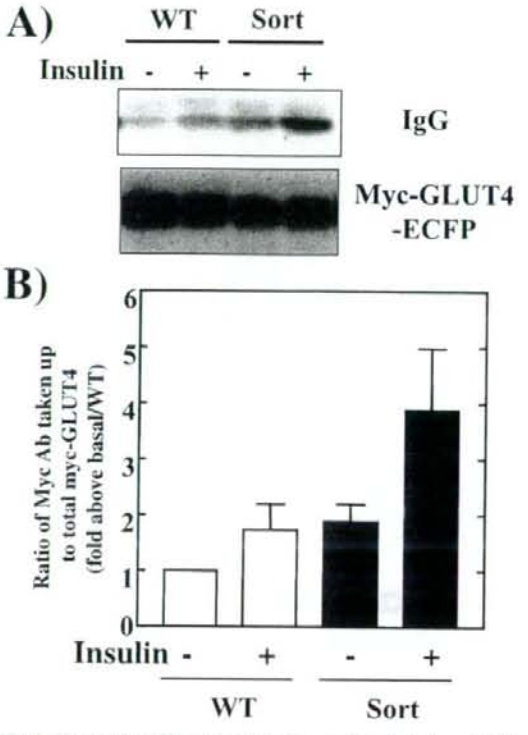

FIGURE 5. **Effect of sortilin overexpression on insulin-induced GLUT4 translocation in C2C12 cells.** *A*, differentiated WT (*open bars*) and Sort10 (*solid bars*) C2C12 myotubes at Day 5 were infected with adenovirus containing the Myc-GLUT4-ECFP gene. Thirty-six hours after infection, the cells were serum starved for 4 h, followed by stimulation with or without 100 nM insulin for 60 min. During the insulin stimulation, 4 μg of anti-Myc antibody was added to the culture. After insulin stimulation, amounts of associated/internalized antibody (*upper panel*) were analyzed by Western blotting. The total amount of Myc-GLUT4-ECFP (*lower panel*) was also analyzed by Western blotting for normalization. *B*, the results of three independent experiments were quantified using ImageJ software. Summarized results were expressed as the mean ± S.E.

myogenesis (Fig. 6). Western blot analysis demonstrated that GLUT1 protein decreased remarkably during differentiation of C2C12 cells (Fig. 6*A*, *left panel, lanes 1, 3,* and *5*). Consistent with our finding that sortilin overexpression suppresses basal glucose uptake (Fig. 4), an obvious reduction of GLUT1 protein was observed in Sort10-C2C12 myoblasts (Fig. 6*A*, *left panel, lane 2*) as compared with that in WT-C2C12 myoblasts (*lane 1*). Upon differentiation, Sort10-C2C12 myotubes displayed marginal levels of GLUT1 protein (Fig. 6*A*, *left panel, lanes 6* and *7*), resulting in lower basal 2-deoxy[^{3}H]glucose uptake than that observed in WT-C2C12 myotubes (Fig. 4*B*). Real-time PCR analysis using a LightCycler (Roche Applied Science) revealed that GLUT1 mRNA expression was significantly decreased in Sort10-C2C12 cells as compared with WT-C2C12 cells even at Day 0 (Fig. 6*B*). Upon differentiation, expression of GLUT1 mRNA reached minimum levels and was present in comparable amounts in WT- and Sort10-C2C12 myotubes on Days 4 and 7 (Fig. 6*B*). We have also confirmed that sortilin overexpression resulted in increased expression of GLUT4 as assessed by both Western blotting (Fig. 6*A*, *right panel*) and real-time PCR analysis (Fig. 6*B*, *right graph*). Because decreased GLUT1 and increased GLUT4 expression are important criteria for myogenesis (43, 44), these data further confirm that sortilin functions as a potent differentiation stimulator in C2C12 cells. It is also noteworthy that, despite the similar expression levels of GLUT1 mRNA in differentiated WT- and Sort10-C2C12 myotubes (Fig. 6*B*, Days 4 and 7), cellular contents of GLUT1 protein were significantly reduced in Sort10-C2C12 (Fig. 6*A*, *lanes 4* and *6*) in comparison with WT-C2C12 (Fig. 6*A*, *lanes 3* and *5*) myotubes.

To assess whether sortilin overexpression alters the stability of GLUT proteins, we next examined time-dependent changes in cellular contents of GLUT1 and GLUT4 in the presence of cycloheximide (Fig. 6*C*). Consistent with a previous report (12), GLUT4 protein displayed greater stability in sortilin-overexpressing C2C12 myoblasts (*right panels*). On the other hand, we found that GLUT1 tended to be less stable in sortilin-overexpressing cells (*left panel*). Taken together, these data indicate that, in addition to the translational regulation, post-transcriptional regulation of GLUT1 protein is also altered by sortilin overexpression.

Increased Ubc9 Expression in Sort10-C2C12 Cells—Cellular contents of GLUT1 and GLUT4 are reportedly regulated post-transcriptionally by exogenous Ubc9 expression in the L6 skeletal muscle cell line (45). We therefore examined expression levels of Ubc9 by Western blotting (Fig. 7*A*) and real-time PCR analysis (Fig. 7*B*) in WT- and Sort10-C2C12 cells during myogenesis. We found that the amount of Ubc9 protein was significantly increased in Sort10-C2C12 cells (Fig. 7*A*, *lanes 2, 4,* and *6*) as compared with WT-C2C12 cells (*lanes 1, 3,* and *5*) at all differentiation time points examined. Consistent with this, a slight increase in Ubc9 mRNA expression was also observed in Sort10-C2C12 cells (Fig. 7*B*, *closed*

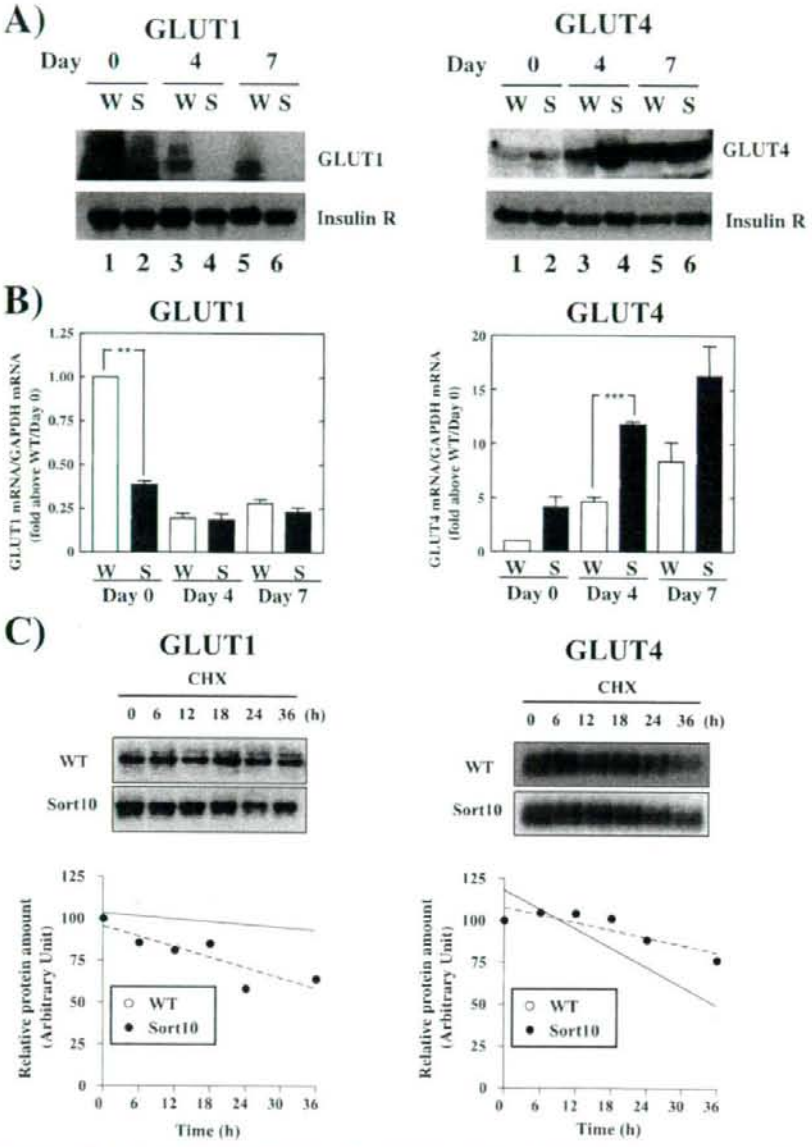

FIGURE 6. **Effect of sortilin overexpression on the protein and mRNA levels of GLUT1 and GLUT4 in C2C12 cells.** *A*, total membrane fractions were obtained from WT-C2C12 cells (*lanes 1, 3,* and *5*) and Sort10-C2C12 cells (*lanes 2, 4,* and *6*) at Day 0 (*lanes 1* and *2*), Day 4 (*lanes 3* and *4*), and Day 7 (*lanes 5* and *6*) of differentiation, as described under "Experimental Procedures." Protein extracts from total membranes (120 μg/lane) were subjected to SDS-PAGE followed by Western blotting using antibodies against GLUT1 (*left panel*) or GLUT4 (*right panel*). *B*, total RNA was isolated from WT-C2C12 cells (*open bars*) and Sort10-C2C12 cells (*solid bars*) on the indicated day after differentiation. The relative abundances of mRNAs for GLUT1 (*left graph*) and GLUT4 (*right graph*) were evaluated by real-time PCR analysis. Data normalized using the glyceraldehyde-3-phosphate dehydrogenase (*GAPDH*) transcript were averaged over three independent experiments and are shown as -fold changes over Day 0 in WT-C2C12 cells. *C*, time dependent changes in protein amounts of GLUT1 (*left panels*) and Myc-GLUT4-ECFP (*right panels*) after addition of 10 μg/ml cycloheximide were monitored in WT (*open circles*) and Sort10 (*closed circles*) C2C12 cells by Western blotting.

bars) as compared with WT-C2C12 cells (*open bars*), whereas expression levels of Ubc9 mRNA decreased upon differentiation in both WT- and Sort10-C2C12 cells. As a result of the increased Ubc9 in Sort10-C2C12 cells, SUMO-modified proteins were also increased (Fig. 7*A*, *right panel*, *lanes 2, 4,* and 6).

DISCUSSION

Although substantial progress has been made in our understanding of the insulin-induced GLUT4 translocation process in adipocytes, achieved mainly using the excellent 3T3L1 adipogenic cell culture model (46), much less information is available about the mechanistic details involved in this event in skeletal muscle, the tissue in which the effect of insulin on glucose disposal is quantitatively most important. Recently, we have reported that, much like the L6 skeletal muscle cell line, a C2C12 myogenic cell line derived from mouse skeletal muscle possesses the basic machinery required for GLUT4 translocation in response to insulin stimulation (43, 47). However, the insulin-induced glucose uptake achieved by this GLUT4 translocation is masked by relatively high basal glucose transport activity, presumably mediated through GLUT1 (35). Because it would be highly desirable to establish cell culture models of skeletal muscle that clearly and accurately reflect muscle glucose disposal *in vivo*, we have attempted to further characterize the molecular details underlying development of the insulin-induced glucose transport system in these C2C12 cells. We therefore explored the functional roles of sortilin, a sorting receptor implicated in the formation of insulin-responsive GLUT4 vesicles in adipocytes (12, 48), by using C2C12 myocytes.

A key finding of the present studies is that sortilin functions as a potent differentiation regulator for C2C12 skeletal muscle cells, at least in part by modulating the p75NTR-proNGF autocrine loop (Figs. 2 and 3). As previously demonstrated in adipocytes (12), sortilin overexpression apparently improves the insulin-induced glucose uptake in C2C12 myocytes (Figs. 4 and 5), a novel observation that, however, reveals that this effect of sortilin on the development of

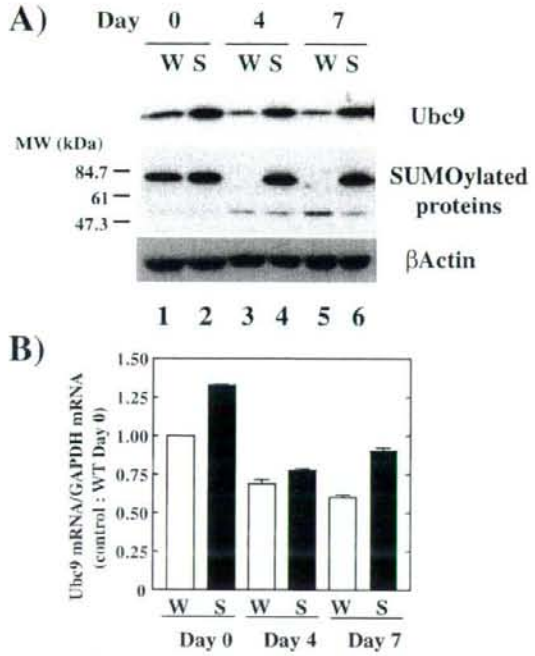

FIGURE 7. **Sortilin overexpression increases Ubc9 resulting in the accumulation of SUMO-modified proteins in C2C12 cells.** *A*, whole cell lysates were obtained from WT-C2C12 cells (*lanes 1, 3,* and *5*) and Sort10-C2C12 cells (*lanes 2, 4,* and *6*) at Day 0 (*lanes 1* and *2*), Day 4 (*lanes 3* and *4*), and Day 7 (*lanes 5* and *6*) of differentiation. Protein extracts (25 μg/lane) were subjected to SDS-PAGE followed by Western blotting using antibodies against anti-Ubc9 (*upper panel*), anti-GMP1 (SUMO-1) (*middle panel*), or anti-β-actin (*lower panel*). *B*, total RNA was isolated from WT-C2C12 cells (*open bars*) and Sort10-C2C12 cells (*solid bars*) on the indicated day after differentiation. The relative abundance of mRNAs for Ubc9 was evaluated by real-time PCR analysis. Data normalized using the glyceraldehyde-3-phosphate dehydrogenase (*GAPDH*) transcript were averaged over three independent experiments and are shown as -fold changes over Day 0 in WT-C2C12 cells.

insulin-responsiveness in C2C12 cells reflects a combination of consequences of its myogenic stimulatory action. Indeed, sortilin overexpression significantly stimulates C2C12 differentiation (Fig. 2) and thereby raises the cellular content of GLUT4 and decreases that of GLUT1 by altering both transcriptional and post-transcriptional levels (Fig. 6). Importantly, the differentiation-dependent expression of endogenous sortilin (Fig. 1) appears to be directly involved in the process of myogenesis, because siRNA-mediated suppression of sortilin significantly inhibited C2C12 differentiation (Fig. 3*C*), which is at least in part mediated through the p75NTR-NGF autocrine loop (Fig. 3*D*). In addition, we found that cellular contents of Ubc9 and SUMO-modified proteins are remarkably increased by sortilin overexpression (Fig. 7). Although it is not clear from the present study whether the up-regulated Ubc9 is directly responsible for post-translational regulation of GLUT proteins as previously reported (45), we observed that GLUT4 became more stable, whereas GLUT1 became less stable, in sortilin-overexpressing C2C12 cells (Fig. 6*C*).

Sortilin Serves as a Stimulator of C2C12 Myogenic Differentiation via Activation of the p75NTR-proNGF Autocrine Loop—In cultured myoblasts, including mouse C2C12 cells and rat L6 cells, serum withdrawal initiates the myogenic differentiation program, and it is generally accepted that autocrine/paracrine actions of insulin-like growth factors in response to serum withdrawal play an important role in the process of muscle differentiation (49, 50). In addition to the insulin-like growth factor-mediated autocrine system, several lines of evidence have demonstrated that NGF, and presumably its unprocessed form termed proNGF, is also involved in the initiation of muscle differentiation in an autocrine fashion (26, 27, 51). Furthermore, overexpression of p75NTR, a low affinity receptor for various neurotrophins, including proNGF, proBDNF, NGF, and BDNF, has been shown to induce spontaneous myogenic differentiation in a growth medium (26), which is similar to what we have observed in C2C12 myoblasts overexpressing sortilin (Fig. 2). Because p75NTR appeared to form a complex with sortilin creating high affinity receptors for proNGF and thereby evoking an intracellular signaling cascade (22), we hypothesized that sortilin overexpression allows endogenous p75NTR to respond to limiting concentrations of neurotrophins being secreted by C2C12 cells in an autocrine manner and/or fed with medium containing fetal bovine serum. Consistent with this idea, neutralizing antibodies against either p75NTR or NGF significantly inhibited the spontaneous differentiation of Sort10-C2C12 cells overexpressing sortilin (Fig. 3*A*). In addition, sortilin overexpression resulted in an efficient endocytosis of the anti-p75NTR antibody from culture media (Fig. 3*B*), suggesting that exogenously expressed sortilin facilitates formation of the functional tripartite complex composed of proNGF, p75NTR, and sortilin, as previously reported (22). More importantly, either siRNA-mediated suppression of endogenous sortilin expression or specific antibody-mediated neutralization of endogenous p75NTR/proNGF significantly inhibits low serum-induced C2C12 differentiation (Fig. 3, *C* and *D*). Together, these data demonstrate that sortilin serves as a stimulator of C2C12 myogenic differentiation mediated through potentiation of the p75NTR-proNGF autocrine loop, and that differentiation-dependent increases in endogenous sortilin participate directly in the promotion of myogenesis. It remains to be clarified whether sortilin has a similar capability in the process of adipocyte differentiation, which is currently under investigation.

It has been reported that sortilin binds mature NGF with low affinity ($K_d = 10^{-8}$ M) and proNGF with high affinity ($K_d = 10^{-9}$ M), and that the latter affinity is further increased ($K_d = 10^{-10}$ M) when sortilin associates with p75NTR (22). Therefore, our data raise the novel possibility that levels of sortilin expression regulate myogenic differentiation by modulating the biological actions mediated through the p75NTR-proNGF autocrine loop. Because sortilin expression is up-regulated (Fig. 1), whereas p75NTR and NGF expressions are down-regulated (26), upon differentiation, fine-tuning of the expression levels of these proteins would be required for proper development and maintenance of healthy muscle tissues (28). Although the signaling cascades involved in its myogenic actions have yet to be clarified, several lines of evidence indicate a signaling relationship between p75NTR and the Rho family of small GTP-binding proteins in the process of cellular differentiation (40,

41). In this regard, regulation of Rho family members has been directly implicated in myogenesis (52, 53), and the inhibition of ROCK by either Y29632 or siRNA-mediated gene silencing reportedly potentiated myogenesis of C2C12 cells (54–56). In the present study, however, we found that Y29632 significantly inhibited the myogenin expression observed in sortilin-overexpressing C2C12 cells early in differentiation (Day 0) (Fig. 3*E*). Since fine-tuning of both Rho family members and ROCK has been shown to be important for myogenesis (54–56), the precise molecular mechanisms underlying the phenomena mentioned above remain to be clarified. However, our results strongly suggest an involvement of ROCK in the potentiation of myogenesis induced by sortilin overexpression.

Effects of Sortilin Expression on the Insulin-responsive Glucose Transport System in C2C12—Sortilin is expressed in a number of tissues, including the brain, testis, and fat, as well as in skeletal muscle and the heart (17, 18, 57). Sortilin has been shown to play an important role in *trans*-Golgi network-to-endosome and *trans*-Golgi network-to-lysosome trafficking events (15). Like cation-independent mannose 6-phosphate/insulin-like growth factor-2 receptor, a well known sorting receptor that traffics among the *trans*-Golgi network, lysosomes, and the plasma membrane, sortilin possesses a short cytoplasmic tail at the C-terminal containing an acidic cluster-dileucine motif that is specifically recognized by the recently identified adaptor proteins termed GGAs (15, 58). In the context of GLUT4 regulation in adipocytes, sortilin expression is up-regulated during 3T3L1 adipocyte differentiation (18, 19), and recent studies by Kandror and colleagues demonstrated a crucial role of sortilin in the formation of insulin-sensitive GLUT4 storage vesicles responsible for the insulin-stimulated glucose transport in 3T3L1 adipocytes (12, 48). Although the precise molecular mechanism involved in the formation of insulin-responsive GLUT4 storage compartments remains largely unknown, the available evidence indicates that sortilin induces the biogenesis of vesicles containing GLUT4 in concert with GGA adaptor proteins in cultured adipocytes (59, 60). More recently, the importance of luminal interactions between sortilin and GLUT4 in endosomes for producing insulin-responsive GLUT4 storage vesicles has been demonstrated (48).

Similar to observations in the 3T3L1 adipogenic cell line (18, 19), our results demonstrate that sortilin is up-regulated upon C2C12 differentiation but is only partially colocalized to GLUT4-containing endosomes (Fig. 1). It should be noted, however, that subcellular organelles underwent a profound reorganization during myogenic differentiation, and their localization patterns and architectures differed remarkably between undifferentiated mononuclear myoblasts and differentiated multinuclear myotubes (8, 61). However, the amount of endogenous sortilin seems to be insufficient for conferring any apparent insulin-responsiveness in terms of glucose uptake in C2C12 myotubes, because insulin stimulation of 2-deoxy[^{3}H]glucose uptake was marginal (Fig. 4*B*), due to a relatively high level of basal glucose uptake mediated through GLUT1. Consistent with previous studies using fibroblastic cell types (12, 48), overexpression of sortilin in myocytes apparently produced insulin-responsiveness as assessed by both the 2-deoxy[^{3}H]glucose uptake assay (Fig. 4) and the Myc Ab uptake assay (Fig. 5). These results support the suggestion of Kandror and colleagues that sortilin plays an essential role in the development of GLUT4 storage vesicles and responsiveness to insulin (12, 48).

However, our aforementioned novel observation that sortilin overexpression significantly potentiates myogenesis sets the stage for an alternative hypothesis that sortilin participates in development of the entire insulin-responsive glucose transport system, being involved in more than just GLUT4 storage compartments, and that this is achieved, at least in part, via its myogenic stimulatory actions. This hypothesis is supported by evidence that sortilin overexpression strongly stimulates expression of the GLUT4 gene while inhibiting that of the GLUT1 gene, leading to opposite changes in GLUT4 and GLUT1 abundance (Fig. 6), which thereby produces lower basal glucose uptake and greater augmentation of glucose uptake in response to insulin (Fig. 4). In addition, emergence of the insulin-responsive glucose uptake in skeletal muscle cells by sortilin overexpression appeared to have resulted, at least in part, from the marked reduction in basal glucose uptake (Fig. 4) due to significantly reduced GLUT1 contents (Fig. 6). In this regard, we observed the half-lives of GLUT proteins to be reciprocally regulated in sortilin-overexpressing C2C12 cells (Fig. 6*C*). Thus, these data indicate sortilin to be involved not only in generating insulin-responsive GLUT4 storage vesicles, but also in elaborating the entire glucose transport system exhibiting enhanced insulin-responsiveness via regulation of the processes of myogenesis including expressions of GLUT proteins and also perhaps various other proteins involved in the development of insulin-responsiveness.

Another interesting observation presented in this study is that sortilin overexpression resulted in significant increases in the contents of Ubc9 and SUMO-modified proteins in C2C12 cells (Fig. 7). Ubc9 is the only protein serving as an E2-type SUMO-conjugating enzyme in vertebrates, and most of the well known Ubc9 interacting proteins are nuclear or are translocated to the nucleus (62, 63). Intriguingly, however, Ubc9 has been shown to interact directly with GLUT1 and GLUT4 and to modulate their membrane expression levels in opposite directions through a post-translational mechanism (45). Namely, overexpression of Ubc9 in the L6 skeletal muscle cell line results in a marked decrease in the cellular GLUT1 content and an increase in the GLUT4 content (45), which is in excellent agreement with our present results, shown in Figs. 6 and 7. Thus, the effects of sortilin overexpression on the significant reduction in cellular GLUT1 content, despite similar expression levels of its gene (Fig. 6, *A* and *B*, Days 4 and 7), may have resulted from the post-translational regulation of GLUT1 governed by the accumulated Ubc9 (Fig. 7). Although possible involvement of the accumulated Ubc9 in the increase in GLUT4 protein is not clear at this time, because it coincides with up-regulation of GLUT4 gene expression in response to sortilin overexpression (Fig. 6, *A* and *B*, *right panels*), a recent

report demonstrated that Ubc9 overexpression results in the inhibition of GLUT4 degradation and promotes its targeting to insulin-responsive GLUT4 storage compartments (64). However, another recent report demonstrated that Ubc9 is also directly involved in the myogenic differentiation of C12C12 cells (65). Thus, Ubc9 seems to have dual functions, and our observations suggest that the sortilin-induced opposite changes in GLUT4 and GLUT1 abundance might reflect a combination of the consequences of the accumulation of Ubc9, which may regulate the half-lives of GLUT proteins and also further participate in the potentiation of myogenesis. Although the degree to which sortilin actions on myogenesis or the opposite changes in GLUT1 and GLUT4 abundance, possibly mediated through Ubc9 accumulation, contributes to enhanced insulin-responsiveness is an important question warranting further research, our findings clearly provide novel insights into the functional roles of sortilin in development of the insulin-responsive glucose uptake system in muscle cells.

Acknowledgments—We thank Dr. H. Shibata (Gunma University) for providing anti-GLUT4 antibody and Dr. H. Mizuguchi (National Institute of Biomedical Innovation) for providing the pHMCA5 plasmid. We also thank Natsumi Emoto and Fumie Wagatsuma for excellent technical assistance.

REFERENCES

1. DeFronzo, R. A., Jacot, E., Jequier, E., Maeder, E., Wahren, J., and Felber, J. P. (1981) *Diabetes* **30,** 1000–1007
2. Nuutila, P., Knuuti, M. J., Raitakari, M., Ruotsalainen, U., Teras, M., Voipio-Pulkki, L. M., Haaparanta, M., Solin, O., Wegelius, U., and Yki-Jarvinen, H. (1994) *Am. J. Physiol.* **267,** E941–E946
3. Koistinen, H. A., and Zierath, J. R. (2002) *Ann. Med.* **34,** 410–418
4. Mueckler, M. (1990) *Diabetes* **39,** 6–11
5. Mitsumoto, Y., Burdett, E., Grant, A., and Klip, A. (1991) *Biochem. Biophys. Res. Commun.* **175,** 652–659
6. Shimokawa, T., Kato, M., Ezaki, O., and Hashimoto, S. (1998) *Biochem. Biophys. Res. Commun.* **246,** 287–292
7. Rodnick, K. J., Slot, J. W., Studelska, D. R., Hanpeter, D. E., Robinson, L. J., Geuze, H. J., and James, D. E. (1992) *J. Biol. Chem.* **267,** 6278–6285
8. Ralston, E., and Ploug, T. (1996) *J. Cell Sci.* **109,** 2967–2978
9. Rudich, A., and Klip, A. (2003) *Acta Physiol. Scand.* **178,** 297–308
10. Garcia de Herreros, A., and Birnbaum, M. J. (1989) *J. Biol. Chem.* **264,** 9885–9890
11. Haney, P. M., Slot, J. W., Piper, R. C., James, D. E., and Mueckler, M. (1991) *J. Cell Biol.* **114,** 689–699
12. Shi, J., and Kandror, K. V. (2005) *Dev Cell* **9,** 99–108
13. Baumann, C. A., Ribon, V., Kanzaki, M., Thurmond, D. C., Mora, S., Shigematsu, S., Bickel, P. E., Pessin, J. E., and Saltiel, A. R. (2000) *Nature* **407,** 202–207
14. Chiang, S. H., Baumann, C. A., Kanzaki, M., Thurmond, D. C., Watson, R. T., Neudauer, C. L., Macara, I. G., Pessin, J. E., and Saltiel, A. R. (2001) *Nature* **410,** 944–948
15. Nielsen, M. S., Madsen, P., Christensen, E. I., Nykjaer, A., Gliemann, J., Kasper, D., Pohlmann, R., and Petersen, C. M. (2001) *EMBO J.* **20,** 2180–2190
16. Lefrancois, S., Zeng, J., Hassan, A. J., Canuel, M., and Morales, C. R. (2003) *EMBO J.* **22,** 6430–6437
17. Petersen, C. M., Nielsen, M. S., Nykjaer, A., Jacobsen, L., Tommerup, N., Rasmussen, H. H., Roigaard, H., Gliemann, J., Madsen, P., and Moestrup, S. K. (1997) *J. Biol. Chem.* **272,** 3599–3605
18. Lin, B. Z., Pilch, P. F., and Kandror, K. V. (1997) *J. Biol. Chem.* **272,** 24145–24147
19. Morris, N. J., Ross, S. A., Lane, W. S., Moestrup, S. K., Petersen, C. M., Keller, S. R., and Lienhard, G. E. (1998) *J. Biol. Chem.* **273,** 3582–3587
20. Nielsen, M. S., Jacobsen, C., Olivecrona, G., Gliemann, J., and Petersen, C. M. (1999) *J. Biol. Chem.* **274,** 8832–8836
21. Mazella, J., Zsurger, N., Navarro, V., Chabry, J., Kaghad, M., Caput, D., Ferrara, P., Vita, N., Gully, D., Maffrand, J. P., and Vincent, J. P. (1998) *J. Biol. Chem.* **273,** 26273–26276
22. Nykjaer, A., Lee, R., Teng, K. K., Jansen, P., Madsen, P., Nielsen, M. S., Jacobsen, C., Kliemannel, M., Schwarz, E., Willnow, T. E., Hempstead, B. L., and Petersen, C. M. (2004) *Nature* **427,** 843–848
23. Teng, H. K., Teng, K. K., Lee, R., Wright, S., Tevar, S., Almeida, R. D., Kermani, P., Torkin, R., Chen, Z. Y., Lee, F. S., Kraemer, R. T., Nykjaer, A., and Hempstead, B. L. (2005) *J. Neurosci.* **25,** 5455–5463
24. Mazella, J. (2001) *Cell Signal* **13,** 1–6
25. Bronfman, F. C., and Fainzilber, M. (2004) *EMBO Rep.* **5,** 867–871
26. Seidl, K., Erck, C., and Buchberger, A. (1998) *J. Cell. Physiol.* **176,** 10–21
27. Erck, C., Meisinger, C., Grothe, C., and Seidl, K. (1998) *J. Cell. Physiol.* **176,** 22–31
28. Reddypalli, S., Roll, K., Lee, H. K., Lundell, M., Barea-Rodriguez, E., and Wheeler, E. F. (2005) *J. Cell. Physiol.* **204,** 819–829
29. Shibata, H., Suzuki, Y., Omata, W., Tanaka, S., and Kojima, I. (1995) *J. Biol. Chem.* **270,** 11489–11495
30. Yaffe, D., and Saxel, O. (1977) *Nature* **270,** 725–727
31. Onishi, M., Kinoshita, S., Morikawa, Y., Shibuya, A., Phillips, J., Lanier, L. L., Gorman, D. M., Nolan, G. P., Miyajima, A., and Kitamura, T. (1996) *Exp. Hematol.* **24,** 324–329
32. Kanzaki, M., Furukawa, M., Raab, W., and Pessin, J. E. (2004) *J. Biol. Chem.* **279,** 30622–30633
33. Mizuguchi, H., and Kay, M. A. (1998) *Hum Gene Ther.* **9,** 2577–2583
34. Mizuguchi, H., and Kay, M. A. (1999) *Hum Gene Ther.* **10,** 2013–2017
35. Nedachi, T., and Kanzaki, M. (2006) *Am. J. Physiol.* **291,** E817–E828
36. Tortorella, L. L., and Pilch, P. F. (2002) *Am. J. Physiol.* **283,** E514–E524
37. Shibata, H., Omata, W., Suzuki, Y., Tanaka, S., and Kojima, I. (1996) *J. Biol. Chem.* **271,** 9704–9709
38. Zeng, J., Hassan, A. J., and Morales, C. R. (2004) *Mol. Reprod. Dev.* **68,** 469–475
39. Peters, E. M., Stieglitz, M. G., Liezman, C., Overall, R. W., Nakamura, M., Hagen, E., Klapp, B. F., Arck, P., and Paus, R. (2006) *Am. J. Pathol.* **168,** 221–234
40. Yamashita, T., and Tohyama, M. (2003) *Nat. Neurosci.* **6,** 461–467
41. Passino, M. A., Adams, R. A., Sikorski, S. L., and Akassoglou, K. (2007) *Science* **315,** 1853–1856
42. Kanzaki, M., and Pessin, J. E. (2001) *J. Biol. Chem.* **276,** 42436–42444
43. Mitsumoto, Y., and Klip, A. (1992) *J. Biol. Chem.* **267,** 4957–4962
44. Santalucia, T., Camps, M., Castello, A., Munoz, P., Nuel, A., Testar, X., Palacin, M., and Zorzano, A. (1992) *Endocrinology* **130,** 837–846
45. Giorgino, F., de Robertis, O., Laviola, L., Montrone, C., Perrini, S., McCowen, K. C., and Smith, R. J. (2000) *Proc. Natl. Acad. Sci. U. S. A.* **97,** 1125–1130
46. Kanzaki, M. (2006) *Endocr. J.* **53,** 267–293
47. Walker, P. S., Ramlal, T., Sarabia, V., Koivisto, U. M., Bilan, P. J., Pessin, J. E., and Klip, A. (1990) *J. Biol. Chem.* **265,** 1516–1523
48. Shi, J., and Kandror, K. V. (2007) *J. Biol. Chem.* **282,** 9008–9016
49. Florini, J. R., Magri, K. A., Ewton, D. Z., James, P. L., Grindstaff, K., and Rotwein, P. S. (1991) *J. Biol. Chem.* **266,** 15917–15923
50. Florini, J. R., Ewton, D. Z., and Coolican, S. A. (1996) *Endocr. Rev.* **17,** 481–517
51. Rende, M., Brizi, E., Conner, J., Treves, S., Censier, K., Provenzano, C., Taglialatela, G., Sanna, P. P., and Donato, R. (2000) *Int. J. Dev. Neurosci.* **18,** 869–885
52. Takano, H., Komuro, I., Oka, T., Shiojima, I., Hiroi, Y., Mizuno, T., and Yazaki, Y. (1998) *Mol. Cell. Biol.* **18,** 1580–1589
53. Charrasse, S., Meriane, M., Comunale, F., Blangy, A., and Gauthier-Rouviere, C. (2002) *J. Cell Biol.* **158,** 953–965
54. Nishiyama, T., Kii, I., and Kudo, A. (2004) *J. Biol. Chem.* **279,** 47311–47319
55. Charrasse, S., Comunale, F., Grumbach, Y., Poulat, F., Blangy, A., and Gauthier-Rouviere, C. (2006) *Mol. Biol. Cell* **17,** 749–759

56. Castellani, L., Salvati, E., Alema, S., and Falcone, G. (2006) *J. Biol. Chem.* **281,** 15249–15257
57. Hermans-Borgmeyer, I., Hermey, G., Nykjaer, A., and Schaller, C. (1999) *Brain Res. Mol. Brain Res.* **65,** 216–219
58. Shiba, T., Takatsu, H., Nogi, T., Matsugaki, N., Kawasaki, M., Igarashi, N., Suzuki, M., Kato, R., Earnest, T., Nakayama, K., and Wakatsuki, S. (2002) *Nature* **415,** 937–941
59. Watson, R. T., Khan, A. H., Furukawa, M., Hou, J. C., Li, L., Kanzaki, M., Okada, S., Kandror, K. V., and Pessin, J. E. (2004) *EMBO J.* **23,** 2059–2070
60. Li, L. V., and Kandror, K. V. (2005) *Mol. Endocrinol.* **19,** 2145–2153
61. Ralston, E. (1993) *J. Cell Biol.* **120,** 399–409
62. Melchior, F. (2000) *Annu. Rev. Cell Dev. Biol.* **16,** 591–626
63. Wilson, V. G., and Rangasamy, D. (2001) *Exp. Cell Res.* **271,** 57–65
64. Liu, L. B., Omata, W., Kojima, I., and Shibata, H. (2007) *Diabetes* **56,** 1977–1985
65. Riquelme, C., Barthel, K. K., Qin, X. F., and Liu, X. (2006) *Exp. Cell Res.* **312,** 2132–2141

Impact of Plasma Oxidized Low-Density Lipoprotein Removal on Atherosclerosis

Yasushi Ishigaki, MD, PhD*; Hideki Katagiri, MD, PhD*; Junhong Gao, MD, PhD*; Tetsuya Yamada, MD, PhD; Junta Imai, MD, PhD; Kenji Uno, MD, PhD; Yutaka Hasegawa, MD, PhD; Keizo Kaneko, MD; Takehide Ogihara, MD, PhD; Hisamitsu Ishihara, MD, PhD; Yuko Sato, PhD; Kenji Takikawa, BA; Norihisa Nishimichi, PhD; Haruo Matsuda, DVM, PhD; Tatsuya Sawamura, MD, PhD; Yoshitomo Oka, MD, PhD

Background—Several clinical studies of statin therapy have demonstrated that lowering low-density lipoprotein (LDL) cholesterol prevents atherosclerotic progression and decreases cardiovascular mortality. In addition, oxidized LDL (oxLDL) is suggested to play roles in the formation and progression of atherosclerosis. However, whether lowering oxLDL alone, rather than total LDL, affects atherogenesis remains unclear.

Methods and Results—To clarify the atherogenic impact of oxLDL, lectin-like oxLDL receptor 1 (LOX-1), an oxLDL receptor, was expressed ectopically in the liver with adenovirus administration in apolipoprotein E–deficient mice at 46 weeks of age. Hepatic LOX-1 expression enhanced hepatic oxLDL uptake, indicating functional expression of LOX-1 in the liver. Although plasma total cholesterol, triglyceride, and LDL cholesterol levels were unaffected, plasma oxLDL was markedly and transiently decreased in LOX-1 mice. In controls, atherosclerotic lesions, detected by Oil Red O staining, were markedly increased (by 38%) during the 4-week period after adenoviral administration. In contrast, atherosclerotic progression was almost completely inhibited by hepatic LOX-1 expression. In addition, plasma monocyte chemotactic protein-1 and lipid peroxide levels were decreased, whereas adiponectin was increased, suggesting decreased systemic oxidative stress. Thus, LOX1 expressed in the livers of apolipoprotein E–deficient mice transiently removes oxLDL from circulating blood and possibly decreases systemic oxidative stress, resulting in complete prevention of atherosclerotic progression despite the persistence of severe LDL hypercholesterolemia and hypertriglyceridemia.

Conclusions—OxLDL has a major atherogenic impact, and oxLDL removal is a promising therapeutic strategy against atherosclerosis. (***Circulation*. 2008;118:75-83.**)

Key Words: atherosclerosis ■ lipoproteins ■ oxidative stress ■ oxidized low-density lipoprotein

Atherosclerosis is the major factor underlying the increased incidence of coronary heart disease and central vascular disease in the industrialized world.[1] Low-density lipoprotein (LDL) cholesterol is considered a major factor in atherosclerosis development.[2] In this decade, several clinical studies of statin therapy have demonstrated the pivotal roles of lowering LDL cholesterol in preventing atherosclerotic progression and decreasing cardiovascular mortality.[3]

Clinical Perspective p 83

Oxidative stress might play critical roles in many diseases. In particular, oxidation of LDL might be a key step in the development of atherosclerosis.[4–6] Oxidized LDL (oxLDL) has been proposed to be involved in many atherogenic changes in the vascular wall such as expression of adhesion molecules, migration of macrophages and smooth muscle cells, release of chemokines,[7] and impairment of endothelial nitric oxide production.[8] Importantly, oxLDL is incorporated into macrophages via receptor-mediated endocytosis, leading to macrophage transformation into foam cells and thus the plaque formation of atherosclerotic lesions. Furthermore, oxLDL itself reportedly induces oxidative stress in endothelial cells, smooth muscle cells, and macrophages, resulting in a vicious cycle of atherogenic plaque formation.[9] However,

Received October 9, 2007; accepted April 18, 2008.

From the Division of Molecular Metabolism and Diabetes (Y.I., J.G., T.Y., J.I., Y.H., K.K., H.I., Y.O.) and Division of Advanced Therapeutics for Metabolic Diseases, Center for Translational and Advanced Animal Research (H.K., K.U., K.K., T.O.), Tohoku University Graduate School of Medicine, Sendai; Department of Vascular Physiology, National Cardiovascular Center Research Institute, Osaka (Y.S., T.S.); and Laboratory of Immunobiology, Department of Molecular and Applied Biosciences, Graduate School of Biosphere Science, Hiroshima University, Hiroshima (K.T., N.N., H.M.), Japan.

*Drs Ishigaki, Katagiri, and Gao contributed equally to this work.

The online Data Supplement, which contains a table, can be found with this article at http://circ.ahajournals.org/cgi/content/full/CIRCULATIONAHA.107.745174/DC1.

Correspondence to Hideki Katagiri, MD, PhD, Division of Advanced Therapeutics for Metabolic Diseases, Center for Translational and Advanced Animal Research, Tohoku University Graduate School of Medicine, 2-1 Seiryo-Machi, Aoba-Ku, Sendai 980-8575, Japan. E-mail katagiri@mail.tains.tohoku.ac.jp

Circulation **is available at http://circ.ahajournals.org** **DOI: 10.1161/CIRCULATIONAHA.107.745174**

the effectiveness of antioxidant therapy against atherosclerosis is controversial.[10–15] In addition, antioxidants may inhibit not only oxLDL formation but also many other oxidation-sensitive pathways. Therefore, it is unclear that the antiatherogenic effects of antioxidants, if any, are due to inhibition of oxLDL formation. Thus, whether lowering oxLDL alone, rather than total LDL, affects atherogenesis remains to be elucidated. Therefore, to directly clarify the impact of oxLDL on the development of atherosclerosis, we designed a strategy for removing oxLDL from the circulation in a murine hypercholesterolemia model: apolipoprotein E (apoE)-deficient mice.

Several receptors for oxLDL have been identified in recent years.[16–20] Lectin-like oxLDL receptor-1 (LOX-1) is one such receptor for oxLDL[21] and is expressed in atherosclerotic lesions, including endothelial cells, macrophages, and smooth muscle cells,[22] suggesting that LOX-1 actively incorporates oxLDL. Therefore, with the goal of removing oxLDL from the circulation, we ectopically expressed LOX-1 in the livers of apoE-deficient mice using an adenoviral gene transfer system.

Methods

Preparation of Recombinant Adenovirus

Recombinant adenovirus containing murine LOX-1 cDNA under the CAG promoter was constructed as described previously.[23,24] A recombinant adenovirus bearing the bacterial β-galactosidase gene (*lacZ*) was used as a control.[25]

Animals

Animal studies were conducted in accordance with the institutional guidelines for animal experiments at Tohoku University. ApoE-deficient mice[26] (The Jackson Laboratory, Bar Harbor, Me) were fed a standard chow. At 46 weeks of age, the baseline group of mice (n=9) were killed to determine the extent of established lesions at this age. Adenoviruses were administered intravenously at a dose of 2×10^8 plaque-forming units to 46-week-old apoE-deficient mice.

Blood Analysis

Plasma total cholesterol, triglyceride, and adiponectin levels were determined as described previously.[27] Plasma lipoproteins were analyzed by high-performance liquid chromatography with molecular sieve columns[28] (Skylight Biotech, Inc, Akita, Japan). The monocyte chemoattractant protein (MCP)-1 concentration was measured with an ELISA kit (R&D Systems, Minneapolis, Minn). Plasma alanine aminotransferase was measured with the transaminase test C (Wako Pure Chemicals, Osaka, Japan). Plasma levels of lipid peroxides were quantified with an LPO determiner (Kyowa Medex, Tokyo, Japan). OxLDL levels were measured with a sandwich ELISA. Murine plasma samples were applied to a plate coated with human soluble LOX-1 protein and detected with anti-apoB as the first antibody and goat anti-chicken IgG (H+L) (KPL, Inc, Gaithersburg, Md) as the detecting antibody. The reaction was developed with a tetramethylbenzidine peroxidase EIA substrate kit (Bio-Rad Laboratories, Hercules, Calif), and absorbance was measured at 450 nm.

Immunoblotting

Hepatic protein extracts (250 μg total protein) were boiled in Laemmli buffer containing 10 mmol/L dithiothreitol, subjected to SDS-PAGE, and transferred onto nitrocellulose filters. The filters were incubated with the murine LOX-1 antibody and then with anti-goat immunoglobulin G coupled to horseradish peroxidase. The immunoblots were visualized with an enhanced chemiluminescence detection kit (Amersham, Buckinghamshire, UK).

Hepatic Uptake of oxLDL

Human LDL ($1.006<d<1.063$ g/mL) was purified by ultracentrifugation and oxidized with $CuSO_4$,[29] followed by labeling with fluorescent lipid (1,1'-dioctadecyl-3,3,3',3'-tetramethylindocarbocyanine perchlorate [DiI]) as described previously.[30] Thirty minutes after DiI-labeled oxLDL (12 μg) injection, murine livers were excised for the extraction of lipids and measurement of fluorescence as described previously,[31] and livers of mice with nonlabeled oxLDL injection also were examined immunohistochemically. Fluorescent intensities of tissue lysates were measured with a fluorescence spectrophotometer (F-2000, Hitachi, Tokyo, Japan).

Histological Analysis

Mouse livers and aortas were removed and rinsed with saline. The tissues were fixed with 10% formalin and embedded in paraffin. Tissue sections were cut at a thickness of 4 μm and stained with hematoxylin and eosin. For immunohistochemistry, the streptavidin-biotin method was performed with a Histofine SAB-PO kit (Nichirei, Tokyo, Japan).[32] Slides were deparaffinized and then autoclaved in citrate buffer for antigen retrieval, followed by incubation with antibodies to oxLDL (Calbiochem, San Diego, Calif), mac-3 (BD Bioscience, San Jose, Calif), and smooth muscle actin (Progen, Heidelberg, Germany). Finally, the slides were visualized by incubation with a substrate solution containing 3,3'-diaminobenzidine tetrahydrochloride.

Measurement of Atherosclerotic Lesions

The aortas were removed, cleaned, cut open with the luminal surface facing up, and then immersion fixed in 10% formalin in PBS. The inner aortic surfaces were stained with Oil Red O to visualize neutral lipid (cholesteryl ester and triglycerides) accumulation for 25 minutes at room temperature. After rinsing with 60% isopropyl alcohol and distilled water, the Oil Red O–stained areas were quantified by Scion Image software analysis (Scion Corp, Frederick, Md) of the digitized microscopic images. Results were expressed as percentages of the lipid-accumulating lesion area to the total aortic area analyzed.

Quantitative Real-Time Polymerase Chain Reaction–Based Gene Expression

On day 5 after adenoviral administration, total RNAs in 0.1 g of the aortas and livers from 24-week-old LacZ and LOX-1 mice were isolated with ISOGEN (Wako Pure Chemical Co, Osaka, Japan), and cDNA was synthesized with a Cloned AMV First Strand Synthesis Kit (Invitrogen, Rockville, Md) using 5 μg total RNA. cDNA synthesized from total RNA was evaluated with real-time quantitative polymerase chain reaction (LightCycler Quick System 350S, Roche Diagnostics GmbH, Mannheim, Germany). The relative amount of mRNA was calculated with GAPDH as the invariant control. The primers used are described in Table I of the online Data Supplement.

Statistical Analysis

All data are expressed as mean±SEM. All statistical analyses were performed with the Statistical Package for the Social Sciences version 13.0 (SPSS Japan Inc, Tokyo, Japan). Normality was tested with the Kolmogorov-Smirnov test. When data were normally distributed, the statistical significance of differences was assessed with the unpaired *t* test and 1-way ANOVA, followed by Tukey's post hoc analyses. The Mann–Whitney *U* test was applied when data were not normally distributed. Repeated-measures ANOVA was used to assess changes in plasma oxLDL values measured serially in time between the 2 experimental groups. In all analyses, values of $P<0.05$ were accepted as statistically significant.

The authors had full access to and take full responsibility for the integrity of the data. All authors have read and agree to the manuscript as written.

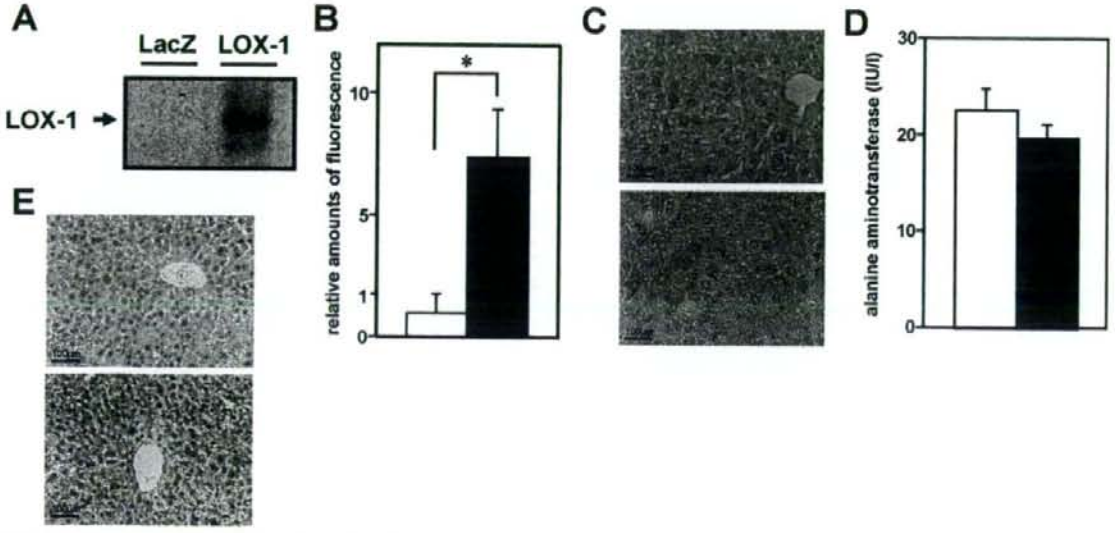

Figure 1. LOX-1 was ectopically and functionally expressed in the liver as an oxLDL receptor. A, Liver extracts were immunoblotted with anti–LOX-1 antibody 5 days after adenoviral administration. B, Mouse livers were removed 30 minutes after intravenous injection of DiI-labeled oxLDL, followed by measurement of fluorescent values in the livers of LacZ mice (white bars) and LOX-1 mice (black bars; n=5 per group). C, The livers of LacZ mice (top) and LOX-1 mice (bottom) were removed 30 minutes after intravenous oxLDL injection, followed by staining of hepatic sections with anti-oxLDL antibody. D, Plasma alanine aminotransferase levels were determined 5 days after adenoviral administration to LacZ mice (white bars) and LOX-1 mice (black bars; n=6 per group). E, The livers of LacZ mice (top) and LOX-1 mice (bottom) were stained with hematoxylin and eosin 4 weeks after adenoviral administration. B, D, Data are presented as mean±SE. *$P<0.05$.

Results

Adenoviruses encoding LOX-1 or LacZ cDNA were administered intravenously to apoE-deficient mice at 46 weeks of age. Mice of this age were chosen because atherosclerosis progresses dramatically during the period just before 1 year of age.[33] As we reported previously,[34] intravenous administration of recombinant adenoviruses results in selective transgene expression in the liver with no detectable expression in other tissues (data not shown). As shown in Figure 1A, administration of LOX-1 adenovirus induced LOX-1 expression in the livers of mice (LOX-1 mice), whereas no LOX-1 expression was detected in those of control mice given LacZ adenovirus (LacZ mice).

To examine hepatic uptake of oxLDL with ectopic expression of LOX-1, fluorescence-labeled oxLDL was injected intravenously, followed by measurement of fluorescence values in the liver. Hepatic fluorescence values were markedly increased in LOX-1 mice compared with LacZ mice (Figure 1B). In addition, 30 minutes after intravenous oxLDL injection, hepatic oxLDL deposition was demonstrated immunohistochemically with anti-oxLDL antibody (Figure 1C). Thus, LOX-1 was ectopically and functionally expressed in the liver as an oxLDL receptor. On the other hand, plasma alanine aminotransferase levels were similar in LacZ- and LOX-1 mice (Figure 1D). In addition, histological analyses revealed no apparent infiltration or structural changes in the livers of LOX-1 mice (Figure 1E). However, hepatic expression of antioxidant enzymes, ie, catalase and glutathione S-transferase, was significantly upregulated (Figure 2A), suggesting increased oxidative stress in hepatocytes. On the other hand, levels of C-reactive protein, interleukin-1β, and tumor necrosis factor-α expression were not significantly altered in the liver (Figure 2B). Thus, LOX-1 ectopically expressed in the livers of apoE-deficient mice functionally incorporated oxLDL into hepatocytes, possibly increasing oxidative stress, but liver damage was apparently limited.

Next, plasma lipid parameters were measured. Hepatic LOX-1 expression did not significantly alter plasma total cholesterol or triglyceride levels (Figure 3A). In addition, cholesterol contents of the LDL and high-density lipoprotein fractions were not significantly altered in LOX-1 mice compared with those in LacZ mice (Figure 3B). In marked contrast, plasma oxLDL levels were dramatically decreased in LOX-1 mice for 2 weeks but returned to control levels by 3 weeks after adenoviral administration (Figure 3C), probably because of decreased adenovirus-mediated transgene expression in the liver after 2 weeks, as reported previously.[27] Thus, adenovirus-mediated LOX-1 expression in the liver resulted in very transient and selective oxLDL removal from the circulation despite the persistence of severe hypercholesterolemia and hypertriglyceridemia induced by apoE deficiency.

To elucidate the effects of hepatic LOX-1 expression on atherosclerosis, the extents of atherosclerotic lesions were determined, as represented by the ratio of Oil Red O–positive areas to the entire aorta. Atherosclerotic lesions of LacZ mice increased markedly, by 38%, during the 4-week period after adenoviral administration (from 46 to 50 weeks of age) compared with those at baseline (46-week-old mice) (Figure 4A and 4B). In contrast, intriguingly, atherosclerotic lesion areas of LOX-1 mice were very similar to those at baseline

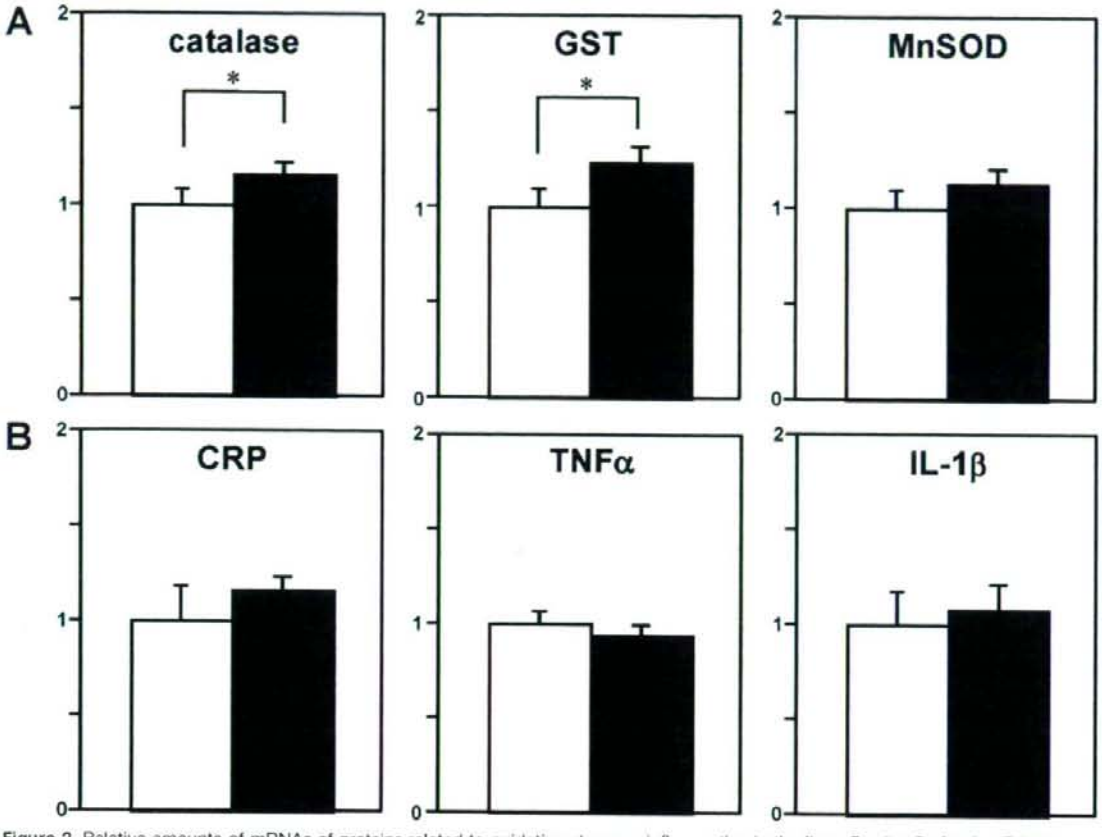

Figure 2. Relative amounts of mRNAs of proteins related to oxidative stress or inflammation in the liver. On day 5 after LacZ (white bars) or LOX-1 (black bars) adenovirus administration to 24-week-old apoE-deficient mice, relative amounts of mRNA of proteins related to oxidative stress (A) or inflammation (B) in the liver were determined by quantitative real-time polymerase chain reaction and corrected with GAPDH as the internal standard (n=9 in LacZ mice, n=11 in LOX-1 mice). Data are presented as mean±SE. GST indicates glutathione S-transferase; MnSOD, manganese superoxide dismutase; CRP, C-reactive protein; TNFα, tumor necrosis factor-α; and IL-1β, interleukin 1β. *$P<0.05$.

and were significantly smaller than those of LacZ mice (Figure 4A and 4B). These findings indicate that hepatic LOX-1 expression completely inhibited the progression of aortic atherosclerosis during the 4-week period when atherosclerosis markedly progresses in control apoE-deficient mice. Thus, oxLDL removal from circulating blood, even transient, exerts striking antiatherogenic effects, indicating the enormous impact of oxLDL on atherosclerosis.

Next, we immunohistochemically examined macrophage and smooth muscle cell infiltration into the plaques. Mac-3 staining revealed that macrophage deposition in established plaque lesions did not differ between LacZ- and LOX-1 mice (Figure 5A and 5B). In contrast, in LOX-1 mice, smooth muscle actin–positive areas in plaques were larger, especially in the surface areas of plaque lesions, than in LacZ mice. In LacZ mice, smooth muscle actin–positive areas in plaques were significantly decreased compared with those at baseline, and these decrements were inhibited by hepatic LOX-1 expression (Figure 5C and 5D). These findings suggest oxLDL removal from the circulation to inhibit the increase in vulnerability that occurs during plaque progression.

Furthermore, plasma MCP-1 levels were significantly lower in LOX-1 mice than in LacZ mice (Figure 6A). In contrast, plasma levels of adiponectin, which is considered a protective molecule against vascular damage,[35] were significantly higher in LOX-1 mice (Figure 6B). In addition, plasma lipid peroxide levels were markedly lower in LOX-1 mice (Figure 6C). Oxidative stress reportedly upregulates and downregulates MCP-1 in vascular cells[36] and adiponectin in adipocytes,[37] respectively. Taken together with the finding of decreased lipid peroxide levels, systemic oxidative stress is likely to be decreased in LOX-1 mice.

Then, we examined mRNA expressions of oxidative stress– and inflammation-related proteins in the aortas of 24-week-old LacZ and LOX-1 mice on day 5 after adenoviral administration. The antioxidant enzymes catalase, glutathione S-transferase, and manganese superoxide dismutase tended to be downregulated in the aortas of LOX-1 mice, although the differences did not reach statistical significance (Figure 7A). In addition, aortic expression of MCP-1, interleukin-6, and interleukin-1β was significantly decreased in LOX-1 mice (Figure 7B), indicating decreased oxidative stress and local

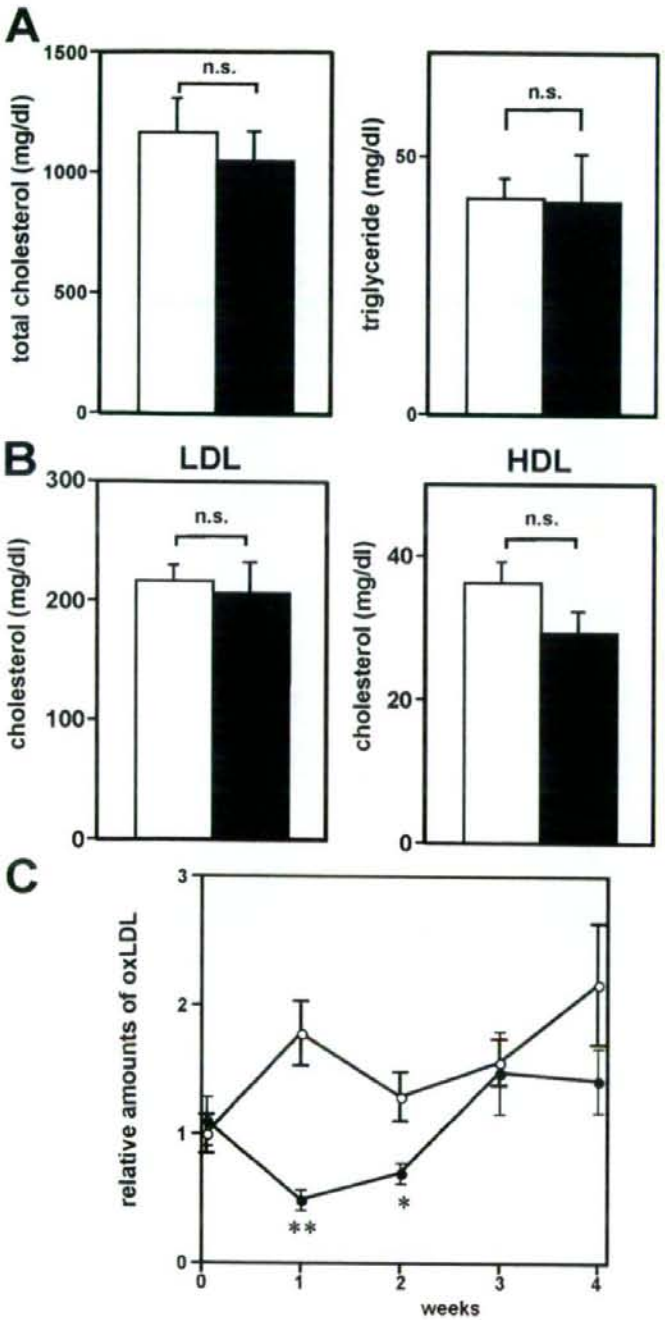

Figure 3. Hepatic LOX-1 expression transiently decreased plasma oxLDL without altering total cholesterol, triglyceride, or LDL cholesterol levels. A, Plasma total cholesterol (left) and triglyceride (right) levels of LacZ mice (white bars) and LOX-1 mice (black bars) were measured after a 10-hour fast 2 weeks after adenoviral administration (n=5 per group). B, Plasma samples (20 μL) from each mouse were separated and analyzed by high-performance liquid chromatography. Cholesterol contents of LDL and high-density lipoprotein (HDL) fractions were determined in LacZ mice (white bars) and LOX-1 mice after a 10-hour fast 2 weeks after adenoviral administration (black bars; n=3 per group). C, Plasma oxLDL levels were determined weekly until 4 weeks after adenoviral administration in LacZ mice (○) and LOX-1 mice (●; n=6 per group). Data are presented as mean±SE. $^{*}P<0.05$, $^{**}P<0.01$.

inflammation in the aortas of LOX-1 mice. OxLDL itself reportedly induces oxidative stress in endothelial cells, smooth muscle cells, and macrophages, resulting in a vicious cycle of atherogenic plaque formation.[9] Taken together, these results show that oxLDL removal from circulating blood may decrease systemic oxidative stress and inflammatory responses by blocking this vicious cycle, thereby exerting further beneficial effects against atherosclerosis.

Discussion

Several clinical studies have shown that lowering LDL cholesterol inhibits the progression of atherosclerosis.[1] The

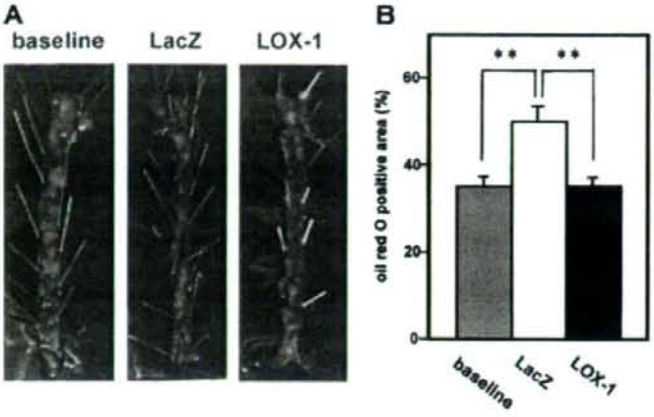

Figure 4. Hepatic LOX-1 expression completely inhibited atherosclerosis progression. A, Aortic atherosclerosis was evaluated as the Oil Red O–positive area. B, The Oil Red O–positive areas were quantified and expressed as percentages of the total aortic area in baseline (46-week-old) mice (gray bars; n=9), 50-week-old LacZ mice (white bars; n=13), and 50-week-old LOX-1 mice (black bars; n=13). Representative histological findings of the whole aorta are shown in A. Data are presented as mean±SE. **$P<0.01$.

beneficial effects of statin therapy for reducing both atherogenic lipoproteins and cardiovascular mortality have been established in this decade. In the present study, despite not altering plasma LDL cholesterol levels, hepatic LOX-1 expression completely inhibited atherosclerotic progression. Thus, oxLDL, but not other LDL fractions, is likely to have a major impact on atherosclerosis development.

In recent reports, LDL cholesterol reduction was shown not only to inhibit coronary atheroma progression[38] but also to induce regression of thoracic aortic plaques, as evaluated by magnetic resonance imaging.[39] Moreover, aggressive lipid-lowering therapy, ie, LDL cholesterol removal, with LDL apheresis produced remarkable regression of coronary atherosclerotic plaques.[40] Here, in LOX-1 mice, atherosclerotic progression was completely inhibited despite a very transient oxLDL decrease, suggesting not only preventive but also therapeutic effects of oxLDL removal. In addition, smooth muscle cells persisted in plaques, particularly in plaque

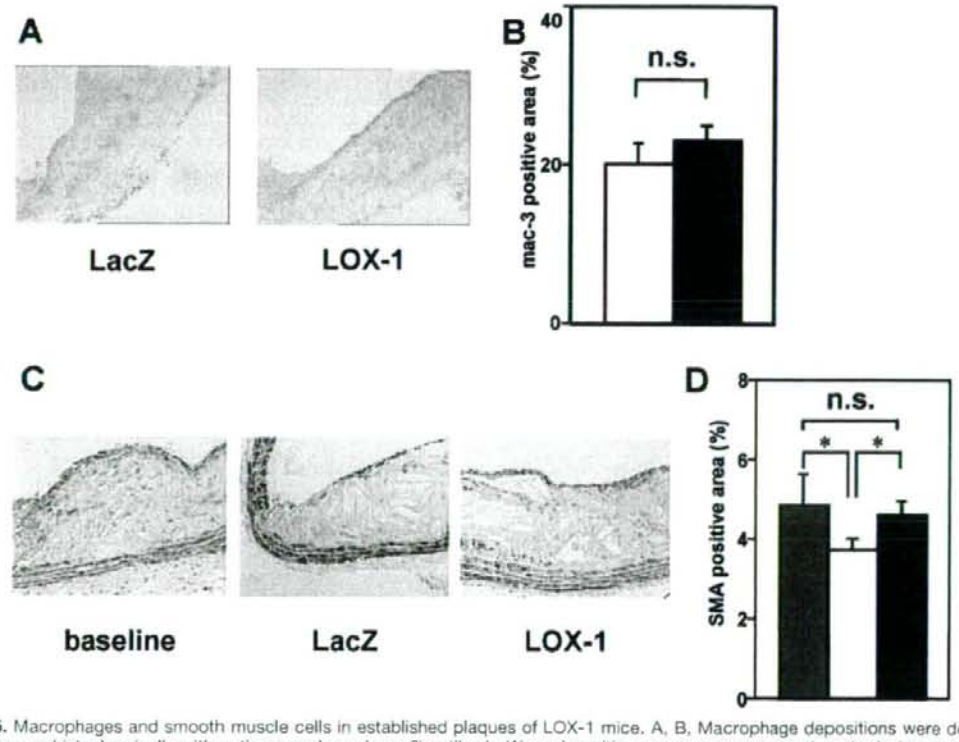

Figure 5. Macrophages and smooth muscle cells in established plaques of LOX-1 mice. A, B, Macrophage depositions were determined immunohistochemically with anti-macrophage (mac-3) antibody (A), and positive areas were measured as the lesion percentage of whole plaques (B). C, D, Smooth muscle cell infiltration was determined immunohistochemically with anti–smooth muscle actin (SMA) antibody (C), and positive areas were measured as the lesion percentage of whole plaques (D). Representative histological findings of the plaque are shown in A and C.

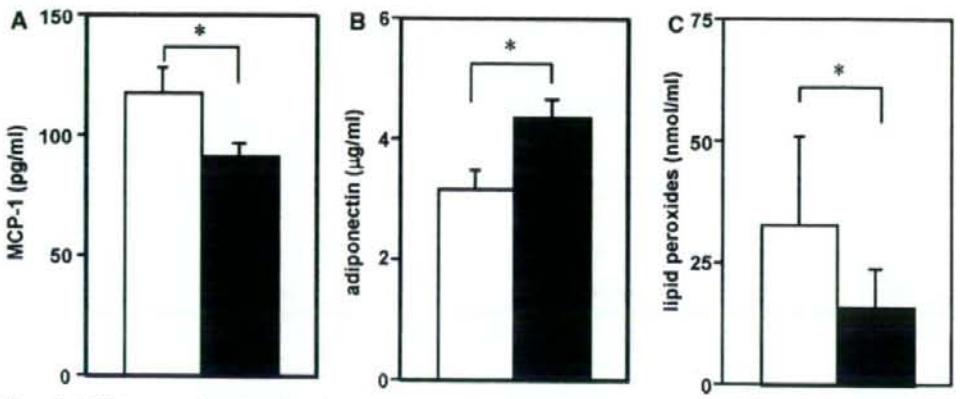

Figure 6. Hepatic LOX-1 expression altered oxidative stress–related plasma parameters. Plasma monocyte chemotactic protein-1 (A), adiponectin (B), and lipid peroxide (C) levels were determined 2 weeks after adenoviral administration to LacZ mice (white bars) and LOX-1 mice (black bars; n=6 per group). Data are presented as mean±SE. *$P<0.05$.

surface areas of LOX-1 mice. OxLDL reportedly enhances apoptosis of smooth muscle cells.[41–43] Therefore, removal of oxLDL from circulating blood may affect the characteristics of plaque lesions by inhibiting apoptosis of smooth muscle cells infiltrating plaque lesions.

Intriguingly, the plasma level of adiponectin, which prevents atherosclerosis development and improves insulin sensitivity, increased with hepatic LOX-1 expression. It was reported that systemic oxidative stress correlates negatively with plasma adiponectin in human subjects[44] and decreases adiponectin expression in adipocytes.[17] On the other hand, plasma MCP-1 levels were suppressed in LOX-1 mice. Oxidative stress may induce MCP-1 upregulation in vascular smooth muscle cells, leading to atherosclerosis formation by

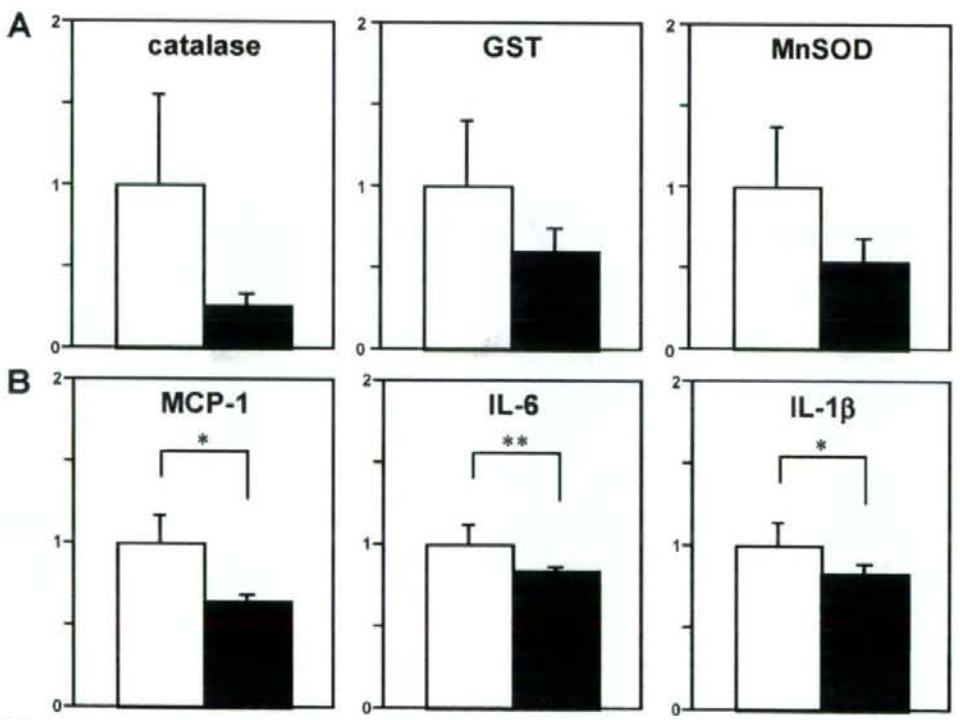

Figure 7. Relative amounts of mRNAs of proteins related to oxidative stress or inflammation in the aorta. On day 5 after LacZ (white bars) or LOX-1 (black bars) adenovirus administration to 24-week-old apoE-deficient mice, relative amounts of mRNA of proteins related to oxidative stress (A) or inflammation (B) in the aorta were determined by quantitative RT-PCR and corrected with GAPDH as the internal standard (n=9 in LacZ mice, n=11 in LOX-1 mice). Data are presented as mean±SE. GST indicates glutathione S-transferase; MnSOD, manganese superoxide dismutase; and IL-6, interleukin-6. *$P<0.05$, **$P<0.01$.

promoting recruitment of inflammatory cells to the vessel wall.[36] We cannot rule out the possibility that LOX-1 expressed in the liver scavenges other pro-oxidant molecules. However, it was reported that oxLDL itself potently induces oxidative stress.[9] Therefore, oxLDL removal from circulating blood is likely to decrease systemic oxidative stress, resulting in adiponectin upregulation and MCP-1 downregulation, thereby exerting further beneficial effects against atherosclerosis.

The effectiveness of antioxidant therapy against atherosclerosis is controversial.[10–15] In murine models, administration of antioxidants effectively reduces atherosclerosis.[12] On the other hand, most clinical trials yielded negative results.[13] This may be at least partly due to insufficient antioxidant effects of natural and synthetic compounds when administered to human subjects. In a randomized placebo-controlled study in healthy adults, daily administration of vitamin E at doses as high as 2 000 mg did not affect the breakdown of lipid peroxidation products despite a substantial increase in plasma vitamin E concentrations.[45] In addition, high doses of these antioxidants reportedly have adverse effects,[15] including the pro-oxidant effects of vitamin E at high doses.[46] Therefore, clinical application of these antioxidants seems to be limited. Thus, the present results provide a potential new therapeutic target because the antiatherogenic effect was observed after transient lowering of oxLDL.

Conclusions

LOX1 expressed in the liver transiently removes oxLDL from circulating blood without altering total cholesterol or LDL cholesterol levels and is likely to decrease systemic oxidative stress, resulting in complete inhibition of atherosclerosis development in aged apoE-deficient mice. This study provides strong evidence of the major atherogenic impact of oxLDL. Removal of oxLDL, even transiently, is a promising therapeutic strategy for blocking the vicious cycle that leads to atherosclerosis.

Acknowledgments

We thank I. Sato, J. Fushimi, K. Kawamura, M. Aizawa, M. Hoshi, and T. Takasugi for technical support.

Sources of Funding

This work was supported by Grants in Aid for Scientific Research (B2, 15390282 to Dr Katagiri and 19591031 to Dr Ishigaki) from the Ministry of Education, Science, Sports and Culture of Japan and by a Grant in Aid for Scientific Research (H19-genome-005) to Dr Oka from the Ministry of Health, Labor, and Welfare of Japan. This work also was supported by two 21st Century COE Programs (to Drs Katagiri and Oka) from the Ministry of Education, Science, Sports, and Culture.

Disclosures

None.

References

1. Katagiri H, Yamada T, Oka Y. Adiposity and cardiovascular disorders: disturbance of the regulatory system consisting of humoral and neuronal signals. *Circ Res*. 2007;101:27–39.
2. Brown MS, Goldstein JL. A receptor-mediated pathway for cholesterol homeostasis. *Science*. 1986;232:34–47.
3. Shepherd J, Cobbe SM, Ford I, Isles CG, Lorimer AR, MacFarlane PW, McKillop JH, Packard CJ. Prevention of coronary heart disease with pravastatin in men with hypercholesterolemia: West of Scotland Coronary Prevention Study Group. *N Engl J Med*. 1995;333:1301–1307.
4. Ross R. Atherosclerosis: an inflammatory disease. *N Engl J Med*. 1999; 340:115–126.
5. Yla-Herttuala S, Palinski W, Rosenfeld ME, Parthasarathy S, Carew TE, Butler S, Witztum JL, Steinberg D. Evidence for the presence of oxidatively modified low density lipoprotein in atherosclerotic lesions of rabbit and man. *J Clin Invest*. 1989;84:1086–1095.
6. Witztum JL, Steinberg D. Role of oxidized low density lipoprotein in atherogenesis. *J Clin Invest*. 1991;88:1785–1792.
7. Yui S, Sasaki T, Miyazaki A, Horiuchi S, Yamazaki M. Induction of murine macrophage growth by modified LDLs. *Arterioscler Thromb*. 1993;13:331–337.
8. Kugiyama K, Kerns SA, Morrisett JD, Roberts R, Henry PD. Impairment of endothelium-dependent arterial relaxation by lysolecithin in modified low-density lipoproteins. *Nature*. 1990;344:160–162.
9. Galle J, Hansen-Hagge T, Wanner C, Seibold S. Impact of oxidized low density lipoprotein on vascular cells. *Atherosclerosis*. 2006;185:219–226.
10. Meagher E, Rader DJ. Antioxidant therapy and atherosclerosis: animal and human studies. *Trends Cardiovasc Med*. 2001;11:162–165.
11. Rimm EB, Stampfer MJ. Antioxidants for vascular disease. *Med Clin North Am*. 2000;84:239–249.
12. Praticò D, Tangirala RK, Rader DJ, Rokach J, FitzGerald GA. Vitamin E suppresses isoprostane generation in vivo and reduces atherosclerosis in ApoE-deficient mice. *Nat Med*. 1998;4:1189–1192.
13. Terasawa Y, Ladha Z, Leonard SW, Morrow JD, Newland D, Sanan D, Packer L, Traber MG, Farese RV Jr. Increased atherosclerosis in hyperlipidemic mice deficient in alpha-tocopherol transfer protein and vitamin E. *Proc Natl Acad Sci U S A*. 2000;97:13830–13834.
14. Dietary supplementation with n-3 polyunsaturated fatty acids and vitamin E after myocardial infarction: results of the GISSI-Prevenzione trial: Gruppo Italiano per lo Studio della Sopravvivenza nell'Infarto miocardico. *Lancet*. 1999;354:447–455.
15. Miller ER 3rd, Pastor-Barriuso R, Dalal D, Riemersma RA, Appel LJ, Guallar E. Meta-analysis: high-dosage vitamin E supplementation may increase all-cause mortality. *Ann Intern Med*. 2005;142:37–46.
16. Kodama T, Freeman M, Rohrer L, Zabrecky J, Matsudaira P, Krieger M. Type I macrophage scavenger receptor contains alpha-helical and collagen-like coiled coils. *Nature*. 1990;343:531–535.
17. Endemann G, Stanton LW, Madden KS, Bryant CM, White RT, Protter AA. CD36 is a receptor for oxidized low density lipoprotein. *J Biol Chem*. 1993;268:11811–11816.
18. Krieger M, Acton S, Ashkenas J, Pearson A, Penman M, Resnick D. Molecular flypaper, host defense, and atherosclerosis: structure, binding properties, and functions of macrophage scavenger receptors. *J Biol Chem*. 1993;268:4569–4572.
19. Acton SL, Scherer PE, Lodish HF, Krieger M. Expression cloning of SR-BI, a CD36-related class B scavenger receptor. *J Biol Chem*. 1994; 269:21003–21009.
20. Ramprasad MP, Terpstra V, Kondratenko N, Quehenberger O, Steinberg D. Cell surface expression of mouse macrosialin and human CD68 and their role as macrophage receptors for oxidized low density lipoprotein. *Proc Natl Acad Sci U S A*. 1996;93:14833–14838.
21. Sawamura T, Kume N, Aoyama T, Moriwaki H, Hoshikawa H, Aiba Y, Tanaka T, Miwa S, Katsura Y, Kita T, Masaki T. An endothelial receptor for oxidized low-density lipoprotein. *Nature*. 1997;386:73–77.
22. Kume N, Murase T, Moriwaki H, Aoyama T, Sawamura T, Masaki T, Kita T. Inducible expression of lectin-like oxidized LDL receptor-1 in vascular endothelial cells. *Circ Res*. 1998;83:322–327.
23. Mizuguchi H, Kay MA. Efficient construction of a recombinant adenovirus vector by an improved in vitro ligation method. *Hum Gene Ther*. 1998;9:2577–2583.
24. Mizuguchi H, Kay MA. A simple method for constructing E1- and E1/E4-deleted recombinant adenoviral vectors. *Hum Gene Ther*. 1999; 10:2013–2017.
25. Katagiri H, Asano T, Ishihara H, Inukai K, Shibasaki Y, Kikuchi M, Yazaki Y, Oka Y. Overexpression of catalytic subunit p110alpha of phosphatidylinositol 3-kinase increases glucose transport activity with translocation of glucose transporters in 3T3-L1 adipocytes. *J Biol Chem*. 1996;271:16987–16990.
26. Zhang SH, Reddick RL, Piedrahita JA, Maeda N. Spontaneous hypercholesterolemia and arterial lesions in mice lacking apolipoprotein E. *Science*. 1992;258:468–471.

27. Ishigaki Y, Katagiri H, Yamada T, Ogihara T, Imai J, Uno K, Hasegawa Y, Gao J, Ishihara H, Shimosegawa T, Sakoda H, Asano T, Oka Y. Dissipating excess energy stored in the liver is a potential treatment strategy for diabetes associated with obesity. *Diabetes*. 2005;54:322–332.
28. Gao J, Katagiri H, Ishigaki Y, Yamada T, Ogihara T, Imai J, Uno K, Hasegawa Y, Kanzaki M, Yamamoto TT, Ishibashi S, Oka Y. Involvement of apolipoprotein E in excess fat accumulation and insulin resistance. *Diabetes*. 2007;56:24–33.
29. Innerarity TL, Pitas RE, Mahley RW. Lipoprotein-receptor interactions. *Methods Enzymol*. 1986;129:542–565.
30. Devaraj S, Hugou I, Jialal I. Alpha-tocopherol decreases CD36 expression in human monocyte-derived macrophages. *J Lipid Res*. 2001; 42:521–527.
31. Fujino T, Asaba H, Kang MJ, Ikeda Y, Sone H, Takada S, Kim DH, Ioka RX, Ono M, Tomoyori H, Okubo M, Murase T, Kamataki A, Yamamoto J, Magoori K, Takahashi S, Miyamoto Y, Oishi H, Nose M, Okazaki M, Usui S, Imaizumi K, Yanagisawa M, Sakai J, Yamamoto TT. Low-density lipoprotein receptor-related protein 5 (LRP5) is essential for normal cholesterol metabolism and glucose-induced insulin secretion. *Proc Natl Acad Sci U S A*. 2003;100:229–234.
32. Yamada T, Katagiri H, Ishigaki Y, Ogihara T, Imai J, Uno K, Hasegawa Y, Gao J, Ishihara H, Niijima A, Mano H, Aburatani H, Asano T, Oka Y. Signals from intra-abdominal fat modulate insulin and leptin sensitivity through different mechanisms: neuronal involvement in food-intake regulation. *Cell Metab*. 2006;3:223–229.
33. Reddick RL, Zhang SH, Maeda N. Atherosclerosis in mice lacking apo E: evaluation of lesional development and progression. *Arterioscler Thromb*. 1994;14:141–147.
34. Uno K, Katagiri H, Yamada T, Ishigaki Y, Ogihara T, Imai J, Hasegawa Y, Gao J, Kaneko K, Iwasaki H, Ishihara H, Sasano H, Inukai K, Mizuguchi H, Asano T, Shiota M, Nakazato M, Oka Y. Neuronal pathway from the liver modulates energy expenditure and systemic insulin sensitivity. *Science*. 2006;312:1656–1659.
35. Okamoto Y, Kihara S, Ouchi N, Nishida M, Arita Y, Kumada M, Ohashi K, Sakai N, Shimomura I, Kobayashi H, Terasaka N, Inaba T, Funahashi T, Matsuzawa Y. Adiponectin reduces atherosclerosis in apolipoprotein E–deficient mice. *Circulation*. 2002;106:2767–2770.
36. Cushing SD, Berliner JA, Valente AJ, Territo MC, Navab M, Parhami F, Gerrity R, Schwartz CJ, Fogelman AM. Minimally modified low density lipoprotein induces monocyte chemotactic protein 1 in human endothelial cells and smooth muscle cells. *Proc Natl Acad Sci U S A*. 1990;87: 5134–5138.
37. Soares AF, Guichardant M, Cozzone D, Bernoud-Hubac N, Bouzaidi-Tiali N, Lagarde M, Geloen A. Effects of oxidative stress on adiponectin secretion and lactate production in 3T3-L1 adipocytes. *Free Radic Biol Med*. 2005;38:882–889.
38. Nissen SE, Tuzcu EM, Schoenhagen P, Brown BG, Ganz P, Vogel RA, Crowe T, Howard G, Cooper CJ, Brodie B, Grines CL, DeMaria AN. Effect of intensive compared with moderate lipid-lowering therapy on progression of coronary atherosclerosis: a randomized controlled trial. *JAMA*. 2004;291:1071–1080.
39. Yonemura A, Momiyama Y, Fayad ZA, Ayaori M, Ohmori R, Higashi K, Kihara T, Sawada S, Iwamoto N, Ogura M, Taniguchi H, Kusuhara M, Nagata M, Nakamura H, Tamai S, Ohsuzu F. Effect of lipid-lowering therapy with atorvastatin on atherosclerotic aortic plaques detected by noninvasive magnetic resonance imaging. *J Am Coll Cardiol*. 2005;45: 733–742.
40. Matsuzaki M, Hiramori K, Imaizumi T, Kitabatake A, Hishida H, Nomura M, Fujii T, Sakuma I, Fukami K, Honda T, Ogawa H, Yamagishi M. Intravascular ultrasound evaluation of coronary plaque regression by low density lipoprotein-apheresis in familial hypercholesterolemia: the Low Density Lipoprotein-Apheresis Coronary Morphology and Reserve Trial (LACMART). *J Am Coll Cardiol*. 2002;40:220–227.
41. Jovinge S, Crisby M, Thyberg J, Nilsson J. DNA fragmentation and ultrastructural changes of degenerating cells in atherosclerotic lesions and smooth muscle cells exposed to oxidized LDL in vitro. *Arterioscler Thromb Vasc Biol*. 1997;17:2225–2231.
42. Nishio E, Arimura S, Watanabe Y. Oxidized LDL induces apoptosis in cultured smooth muscle cells: a possible role for 7-ketocholesterol. *Biochem Biophys Res Commun*. 1996;223:413–418.
43. Okura Y, Brink M, Itabe H, Scheidegger KJ, Kalangos A, Delafontaine P. Oxidized low-density lipoprotein is associated with apoptosis of vascular smooth muscle cells in human atherosclerotic plaques. *Circulation*. 2000; 102:2680–2686.
44. Furukawa S, Fujita T, Shimabukuro M, Iwaki M, Yamada Y, Nakajima Y, Nakayama O, Makishima M, Matsuda M, Shimomura I. Increased oxidative stress in obesity and its impact on metabolic syndrome. *J Clin Invest*. 2004;114:1752–1761.
45. Meagher EA, Barry OP, Lawson JA, Rokach J, FitzGerald GA. Effects of vitamin E on lipid peroxidation in healthy persons. *JAMA*. 2001;285: 1178–1182.
46. Bowry VW, Ingold KU, Stocker R. Vitamin E in human low-density lipoprotein: when and how this antioxidant becomes a pro-oxidant. *Biochem J*. 1992;288(pt 2):341–344.

CLINICAL PERSPECTIVE

A consensus has been reached that lowering plasma low-density lipoprotein (LDL) inhibits atherosclerosis progression. However, whether lowering plasma oxidized LDL (oxLDL) alone contributes to preventing atherosclerosis remains uncertain. The antiatherogenic effects of antioxidant therapy that may inhibit oxLDL formation are controversial because most clinical trials yielded negative results. Here, it has been shown that removal of oxLDL from the circulation has a very strong effect against atherosclerosis. In this study, lectin-like oxLDL receptor 1 (LOX-1), an oxLDL receptor, was expressed ectopically in the livers of apolipoprotein E–deficient mice (LOX-1 mice), using adenoviral gene transfer, to remove oxLDL from the circulation. Intriguingly, a transient decrease in plasma oxLDL, without affecting non-oxLDL cholesterol levels, completely inhibited atherosclerotic progression. Systemic oxidative stress was shown to be decreased in LOX-1 mice. Thus, oxLDL plays very important roles in atherosclerosis formation, and the underlying mechanisms may involve both direct (foam cell formation) and indirect (increased oxidative stress) effects. In addition, smooth muscle cells in the surface areas of atherosclerotic plaques were increased in LOX-1 mice, suggesting that oxLDL makes plaques vulnerable, possibly leading to plaque ruptures. Thus, the results of this study provide potential therapeutic targets for atherosclerosis, ie, treatments that would potently lower plasma oxLDL, including inhibition of oxLDL formation and removal of oxLDL from the circulation. These promising strategies may contribute to the prevention of not only atherosclerosis formation but also the development of acute coronary syndrome.